Knowledge models for the engineering and optimization of photobioreactors

Jeremy Pruvost, Jean-François Cornet

Jérémy Pruvost and Jean-François Cornet

10 Knowledge models for the engineering and optimization of photobioreactors

10.1 Introduction

The modeling of microalgal photosynthetic biomass production draws some support from the abundant literature on bioprocess modeling, in particular when mineral or CO_2 mass-transfer limitations on growth rates are considered in the same way as substrate and O_2-transfer limitations in engineered bacterial cultivation. However, photosynthetic biomass growth exhibits highly specific features owing to its need for light energy: unlike dissolved nutrients, assumed to be homogeneous in well-mixed conditions, light energy is heterogeneously distributed in the culture due to absorption and scattering by cells, independently of the mixing conditions. As light is the principal energy source for photosynthesis, this heterogeneity alone sets microalgal cultivation systems apart from other classical bioprocesses, as they are generally limited by light transfer inside the culture media. Hence the design, optimization and control of photobioreactors (PBRs) require specific approaches.

This chapter deals with developing useful knowledge models for engineering microalgal cultivation systems. Prerequisites and main concepts will be presented. Concrete illustrations will be given that use modeling to gain a deeper understanding of the complex influence of light transfer on the process, and to predict biomass productivities as a function of cultivation system engineering variables (especially depth of culture) and operating settings (residence time and incident light flux) in both artificial constant light and natural sunlight conditions.

10.2 Theoretical background for radiation measurement and handling

10.2.1 Main physical variables

Given the crucial importance of radiative transfer description in photobioreactor modeling, it is essential to have a broad overview of the main physical quantities and definitions involved in radiation measurement and theory, together with a thorough knowledge of the conversion factors linking the two main practical systems of units (joules and micromoles of photons). There is often much confusion on these points in the microalgal growth modeling literature, conducive to misinterpretation of related physical and physiological processes. This section gives a

brief summary of the definitions, units, roles and related sensors for the three main useful physical quantities in the field of PBR modeling.

Strictly speaking, these three quantities are all spectral quantities (their definition holds for a small differential part of the electromagnetic spectrum $\mathrm{d}\lambda$ indicated by a subscript λ), but for simplicity, in what follows we will mainly consider mean averaged quantities for photosynthetically active radiation (PAR). Thus the absence of an λ subscript means that we are working with integral quantities such as $X = \int_{\Delta\lambda} X_\lambda \,\mathrm{d}\lambda$, in which $\Delta\lambda$ corresponds to the range of wavelengths between 400 and 700 nm (PAR).

The first measurable variable (defined from an elemental oriented surface of reference $\mathrm{d}S$) from which all the other useful and practical radiative quantities are deduced is the radiance, more generally named intensity I in many fields of physics (see Fig. 10.1). It is the ratio, in a given direction, of the solid angle $d\mathbf{\Omega}$ and in a point of the oriented surface $\mathrm{d}S$ of the radiant power $\mathrm{d}E$ to the projected area on the perpendicular plane to the outward normal **n**:

$$I = \frac{\mathrm{d}E}{\mathrm{d}S\cos\Theta} \quad \left[\mathrm{W.sr^{-1}.m^{-2}} \text{ or } \mu\mathrm{mol}_{h\upsilon}.\mathrm{s^{-1}.sr^{-1}.m^{-2}}\right] \tag{10.1}$$

This fundamental directional quantity may be integrated over the solid angle $\mathrm{d}\omega$, giving the definition of the radiative flux density **q** such that the flux through an elemental surface $\mathrm{d}S$ of normal **n** is $\mathbf{q} \cdot \mathbf{n}\, dS$.

In a given direction x, the projection of **q** is then:

$$q_x = \iint_{4\pi} I\cos\Theta\,\mathrm{d}\omega = \int_0^{2\pi}\int_0^{\pi} I\cos\Theta\sin\Theta\;\mathrm{d}\Theta\;\mathrm{d}\Phi \qquad \left[\mathrm{W.m^{-2}} \text{ or } \mu\mathrm{mol}_{h\upsilon}.\mathrm{s^{-1}.m^{-2}}\right] \tag{10.2}$$

where $\cos\Theta$ is the angle between the outward normal **n** and the considered direction **Ω** (see Fig. 10.1), so defining the vectorial nature of this quantity.

In the field of PBR modeling, this flux density is mainly used to define the boundary conditions relative to given illumination conditions. In this case, only the incoming radiation on one hemisphere that penetrates the culture medium is of interest, giving the definition of the incident hemispherical radiant flux density or photon flux density (PFD) perpendicular to a reference surface:

$$q_0 = \int_0^{2\pi}\int_0^{\pi/2} I_0\cos\Theta\sin\Theta\,\mathrm{d}\Theta\,\mathrm{d}\Phi \tag{10.3}$$

We note that the angular nature of this PFD may be different, and in some cases (especially for solar illumination) it may be useful to use a subscript to characterize this flux, such as $q_{//}$ for a collimated incidence, $q_\perp$ for the special case of normal collimation or $q_\cap$ for diffuse incidence. In all cases, this hemispherical radiant flux

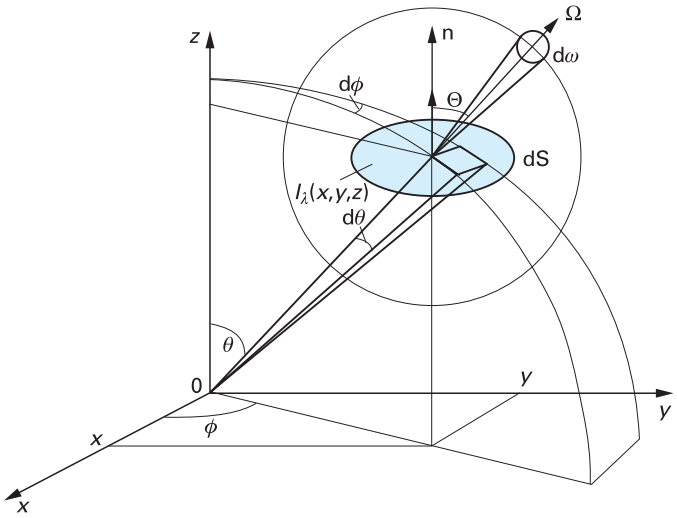

Fig. 10.1: Definition of the solid angle dω and of the associated intensity (strictly, radiance) $I_\lambda(x, y, z, \Theta, \Phi)$ from a fixed Cartesian $\mathbf{r}(x, y, z)$ or spherical $\mathbf{r}(r, \theta, \varphi)$ frame of reference associated with a moving frame $\Omega(\Theta, \Phi)$ at a point P from which it is possible to derive all the radiative useful integral definitions for the description of radiative transfer in photobioreactor modeling.

density component can be measured with a flat cosine sensor, once a surface of reference has been chosen (Pottier et al. 2005).

The third and last integral quantity of interest, mainly to define the total radiant light energy available for photosynthesis and then formulate the kinetic and energy couplings, is the scalar spherical irradiance:

$$G = \iint_{4\pi} I \, \mathrm{d}\omega = \int_0^{2\pi} \int_0^{\pi} I \sin\Theta \, \mathrm{d}\Theta \, \mathrm{d}\Phi \quad (\mathrm{W.m^{-2}} \text{ or } \mu\mathrm{mol_{h\nu}.s^{-1}.m^{-2}}) \tag{10.4}$$

This quantity can be evaluated with a spherical quantum sensor, which strictly measures an energy fluence rate, assumed to be the irradiance if the sensor diameter is small compared with the characteristic extinction length for the radiation in the considered medium (Pottier et al. 2005).

We note that for modeling purposes, the angular pattern of the light must necessarily be known, to calculate the integrals of Equations (10.3) and (10.4) but is extremely difficult to measure. It can be postulated a priori or calculated from models of radiative emission. In all cases, this angular distribution ranges between two extremes:

– A collimated radiation giving the following relations between I_0, q_0 and G_0:

$$q_0 = q_{//} = \int_0^{2\pi} \int_0^{\pi/2} I_0^{col} \delta(\Theta - \Theta_{col}) \delta(\Phi - \Phi_{col}) \cos\Theta \sin\Theta \, d\Theta \, d\Phi = I_0^{col} \cos\Theta_{col}$$

$$= G_0 \cos\Theta_{col}$$

– A diffuse isotropic radiation for which:

$$q_0 = q_\cap = I_0^{dif} \int_0^{2\pi} \int_0^{\pi/2} \cos\Theta \sin\Theta \, d\Theta \, d\Phi = 2\pi \frac{1}{2} I_0^{dif} = \pi I_0^{dif} = \frac{G_0}{2}$$

10.2.2 Solar illumination

As previously defined, the light energy received by a solar cultivation system is represented by the hemispherical incident light flux density q, or photon flux density (PFD), which has to be expressed within the range of photosynthetic active radiation (PAR), i.e. the 0.4–0.7 µm bandwidth. For example, the whole solar spectrum at ground level covers the range 0.26–3 µm. The PAR range thus corresponds to almost 43 % of the full solar energy spectrum (for AM = 1.5 normalization).

As light is converted inside the culture volume, it is also necessary to add to the PFD determination a rigorous treatment of radiative transfer inside the culture (see later on in this chapter) strictly requiring knowledge of the angular distribution of the incoming light, together with the light-source positioning with respect to the optical transparent surface of the cultivation system, i.e. the incident polar angle θ (Fig. 10.2). Ideally, collimated (direct) $q_{//}$ and diffuse $q_\cap$ components of radiation should be considered separately. By definition, the direction of a beam of radiation, which represents direct radiation received from the light source, will define the incident polar angle θ with the illuminated surface and the direct light flux density $q_{//}$. By contrast, diffuse radiation cannot be defined by a single incident angle but has an angular distribution over the illuminated surface (on a 2π solid angle for a plane). Because this angular distribution is unknown, an isotropic angular distribution (Lambertian behavior) is generally assumed when using the value of $q_\cap$.

10.3 Modeling light-limited photosynthetic growth in photobioreactors

10.3.1 Overview of the modeling approach

The photosynthetic activity (here represented by the specific oxygen production rate J_{O_2}) is directly related to the local light available inside the culture medium. This is usually represented by the light-response curve (Fig. 10.3). This curve is

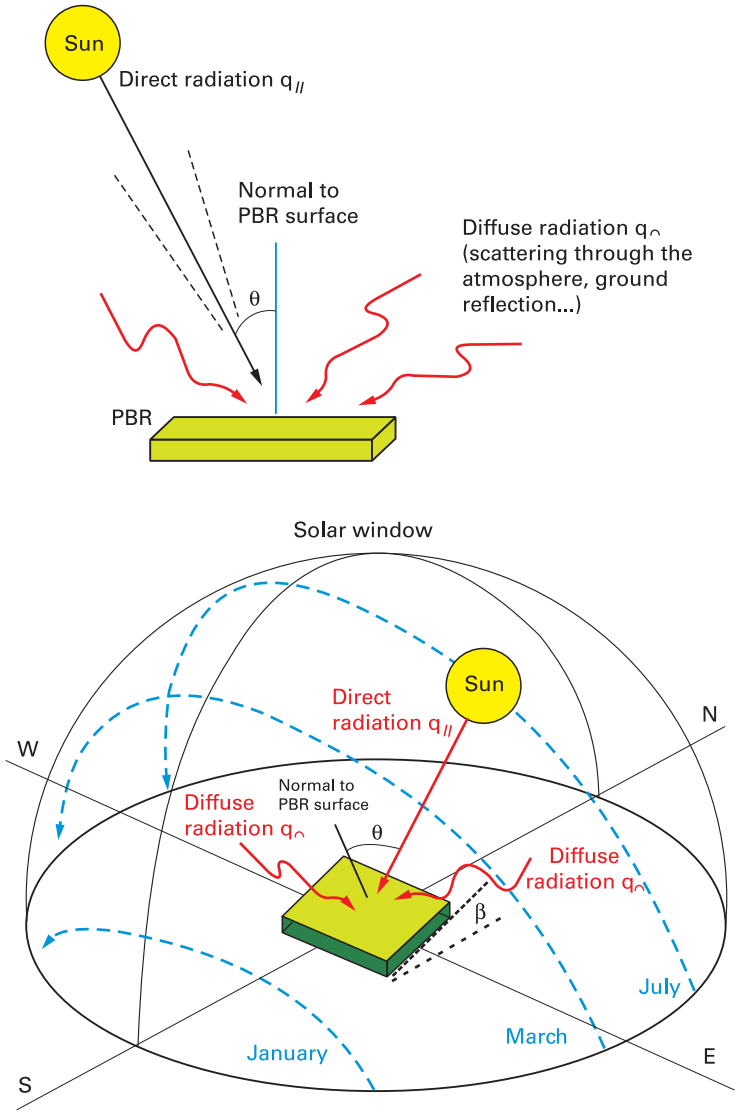

Fig. 10.2: Solar radiation on a microalgal cultivation system: incident angle and diffuse-direct radiations (left), time course of solar sky path during the year (right).

characterized by progressive saturation of photosynthesis with irradiance G up to an irradiance of saturation G_s. For higher irradiances, photoinhibition processes can occur with a negative influence on growth (Vonshak and Torzillo 2004). We also note that a threshold value of irradiance is needed to obtain positive growth. This value is termed the irradiance of compensation G_C (corresponding to the

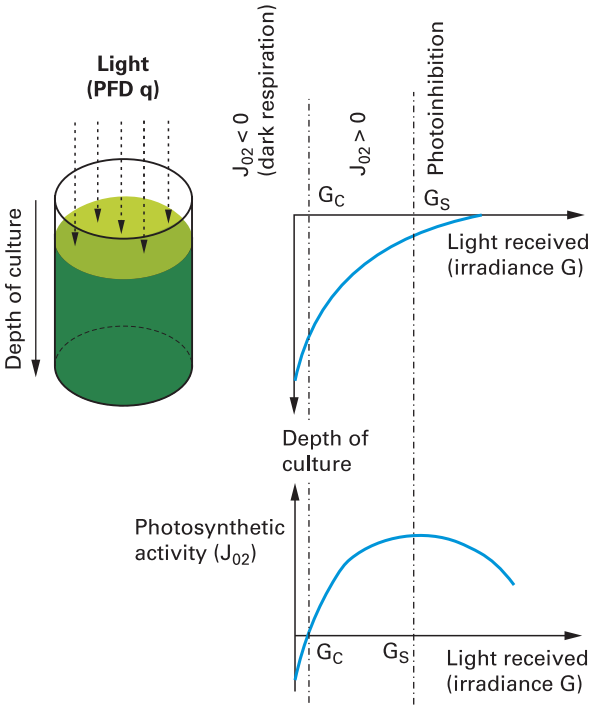

Fig. 10.3: Relation between light attenuation and photosynthetic growth in microalgal cultivation systems.

"compensation point of photosynthesis"), which will prove relevant in the modeling and understanding of PBR operation (see later on in this chapter).

In cultivation systems, this nonlinear, complex response of photosynthesis has to be considered in combination with the light-attenuation conditions. In extreme cases of high light illumination and high light attenuation (high biomass concentration), cells in different physiological states will co-occur: some, close to the light source, may be photoinhibited, while others deep in the culture will receive no light. Ideally, the control of the system would require taking all these processes into account, a far from trivial task. As described next, modeling the kinetic coupling of photosynthetic growth with the radiation field inside cultivation systems will enable us to represent the impact of such effects on process efficiency. The main features of such a model are presented in the following sections.

10.3.2 Mass balances

The mass balance relates concentration in the cultivation system to kinetic rates of biological production (biomass, O_2) or consumption (nutrients, CO_2) and system

input and output. For a continuous system, assuming perfectly mixed conditions (continuous stirred tank reactor or CSTR model), the concentration C of a given element is then given by (Cornet et al. 2003; Pruvost et al. 2008; Pruvost 2011):

$$\frac{dC}{dt} = \langle r(t) \rangle + \frac{1}{\tau}(C_i - C) = \langle r(t) \rangle + D\ (C_i - C) \tag{10.5}$$

with <r> the mean volumetric production (biomass, metabolites) or consumption (nutrient) rate in the system, and τ the residence time resulting from the liquid flow rate of the feed of input concentration C_i (fresh medium) (with $\tau = 1/D$, where D is the dilution rate).

Following the CSTR model, Equation (10.5) assumes homogeneous concentration in the cultivation system. Because of the slow growth rate of photosynthetic microorganisms compared with mixing time, this is usually the case, and so Equation (10.5) holds. In some cases of large tubular cultivation systems without recycling, it may be necessary to work with the steady-state plug flow tubular reactor (PFTR) model, assuming a constant concentration only on a cross-section of the tube:

$$u_x \frac{dC}{dx} - D_L \frac{d^2C}{dx^2} = \langle r(x) \rangle \tag{10.6}$$

with u_x the linear velocity obtained along the flowing x-axis ($u_x = Q/S$ with Q the liquid flow rate and S the tubular cross-section) and D_L the axial dispersion coefficient. This equation represents the evolution of concentration as a function of the distance x (length of the tube).

10.3.3 Stoichiometry of photosynthetic growth

10.3.3.1 Simple stoichiometric equations

Growth can be expressed in the form of a stoichiometric equation that can be deduced, for example, from a biomass elemental analysis (Roels 1983). As for bacteria, the stoichiometric equation for photosynthetic growth in optimal conditions is found to be largely independent of the cultivated species, and depends only weakly on illumination and radiation field conditions (nutrient starvation can, by contrast, strongly influence biomass composition (Pruvost et al. 2011a)). Below are two examples for *Chlamydomonas reinhardtii* (Eq. (10.7)) and *Arthrospira platensis* (Eq. (10.8)), emphasizing the difference in the photosynthetic quotient $Q_P = \upsilon_{O_2-CO_2}$ due to the nitrogen source (ammonium for *C. reinhardtii vs.* nitrate for *A. platensis*), which is found to have the greatest impact on stoichiometric equation and redox balance, rather than the C-molar formula itself:

$$CO_2 + 0.593\ H_2O + 0.176\ NH_3 + 0.007\ H_2SO_4 + 0.018\ H_3PO_4 \rightarrow CH_{1.781}O_{0.437}N_{0.176}S_{0.007}P_{0.018} + 1.128\ O_2 \quad (10.7)$$

$$CO_2 + 0.71\ H_2O + 0.14\ HNO_3 + 0.008\ H_2SO_4 + 0.005\ H_3PO_4 \rightarrow CH_{1.59}O_{0.55}N_{0.14}S_{0.008}P_{0.005} + 1.32\ O_2 \quad (10.8)$$

As for any biological production, a stoichiometric equation is useful for converting biomass growth rates into substrate or product rates, for example to determine nutrient requirements (especially in terms of nitrogen, phosphorus and sulfur sources for photosynthetic microorganisms). It is also practically useful for understanding the CO_2 / O_2 exchange and mass-transfer limitations or the CO_2-related pH time course when the stoichiometric equation is expressed by the charge of ionic species (Cornet et al. 1998)

10.3.3.2 Structured stoichiometric equations

More sophisticated structured equations can be developed if a deep understanding of the coupling between energetics, kinetics and stoichiometry in the photosynthesis process at the cell level is sought (Roels 1983). These equations involve the stoichiometric cofactor balances such as $NADPH,H^+$ in photosynthesis and the associated ATP production rate defining the $P / 2e^-$ ratio in the Z-scheme of photosynthesis (Cornet et al. 1998). For example, in the case of *A. platensis* growth, the stoichiometric equation (Eq. (10.8)) may be rewritten, from a structured analysis of the $P / 2e^-$ ratio for each main cellular component (proteins, lipids, carbohydrates, etc.), and for a mean value of the incident PFD of 500 $\mu mol_{h\nu}.m^{-2}.s^{-1}$ as:

$$CO_2 + 1.71\ H_2O + 0.14\ HNO_3 + 0.008\ H_2SO_4 + 3.62\ ATP + 2.62\ (NADPH, H^+) \xrightarrow{J_X} CH_{1.59}O_{0.55}N_{0.14}S_{0.008}P_{0.005} + 3.61\ P_i + 3.62\ ADP + 2.62\ NADP^+ \quad (10.9)$$

This equation can be associated with the corresponding stoichiometric pair of structured equations for the Z-scheme of photosynthesis:

$$2.62\ NADP^+ + 2.62\ H_2O \xrightarrow{J_{NADPH_2}} 2.62\ (NADPH, H^+) + 1.32\ O_2$$
$$3.62\ (ADP + P_i) \xrightarrow{J_{ATP}} 3.62\ ATP + 3.62\ H_2O \quad (10.10)$$

the sum of which corresponds to the previous non-structured stoichiometry (Eq. (10.8)). In this particular example with mean illumination conditions, the $P/2e^-$ ratio of the cells yields:

$$P / 2e^- = \frac{J_{ATP}}{J_{NADPH_2}} = 1.38 \quad (10.11)$$

Knowing this ratio is most useful, as it enables us to calculate the stoichiometric molar quantum yield for the reaction φ'_X (i.e. considering only the "conservative" photons linked to the electron transfers coming from water oxidation) from the definition (Cornet and Dussap 2009):

$$\varphi'_X = \frac{1}{2\upsilon_{NADPH,H^+-X}(1 + P/2e^-)} \tag{10.12}$$

which emerges as an important parameter in the kinetic coupling model (see later on in this chapter). Most importantly, we note that this quantum yield has been shown to be weakly dependent on the radiation field because of antagonistic effects in the $P/2e^-$ and υ_{NADPH,H^+-X} deviations in Equation (10.12), and because its theoretical calculation (Cornet 2007) requires averaging fast kinetic rates over a period of time corresponding roughly to the circulation time in the PBR. Thus it may be considered as a mean constant value representative of the photon efficiency for a given N-source. In the present case for nitrate, this mean molar quantum yield is:

$$\overline{\varphi}'_X \cong 8 \times 10^{-8}\,\mathrm{mol}_X.\mu\mathrm{mol}_{h\upsilon}^{-1} \tag{10.13}$$

The same reasoning applied with ammonia as N-source gives:

$$\overline{\varphi}'_X \cong 1 \times 10^{-7}\,\mathrm{mol}_X.\mu\mathrm{mol}_{h\upsilon}^{-1} \tag{10.14}$$

thus demonstrating that photosynthesis on ammonia is 25 % more efficient than on nitrate.

If necessary, these molar quantum yields can be converted into mass quantum yields ($\mathrm{kg}_X.\mu\mathrm{mol}_{h\upsilon}^{-1}$), providing the C-molar mass of any given microorganism $M_X \cong 0.024$ kg/C-mol$X$ (to be determined exactly from the C-molar formula of biomass), or in molar and mass energy yields ($(\mathrm{mol}_X$ or $\mathrm{kg}_X).\mathrm{J}^{-1}$) from a conversion factor linking moles of photons to joules (e.g. 4.6 $\mu\mathrm{mol}_{h\upsilon}$/J in solar illumination).

10.3.4 Kinetic modeling of photosynthetic growth

Solving the mass balance equation for a given compound (Eq. (10.5) or (10.6)) involves determining the mean volumetric production (or consumption) rate $\langle r \rangle$. In bioprocesses, this rate results from biological reactions and is linked to all the possible limitations that can occur in the cultivation system. Our discussion will focus here on light limitation. This is a specific feature of photosynthetic microorganism cultivation, and because of the high light demand, most cultivation systems are (at least) light-limited. As will be shown later, strictly light-limited condi-

tions will also afford the best productivity. If needed, other limitations can obviously be considered (growth limitation by inorganic carbon or mineral nutrient concentration, temperature influence, etc.). This requires appropriate kinetic relations, and the interested reader can refer to Fouchard et al. (2009), where both light and nutrient limitations were modeled in the particular case of sulfur deprivation, which leads to hydrogen production by *C. reinhardtii*.

Photosynthetic growth can be expressed first from the local specific rate of oxygen production or consumption J_{O_2}, considered here at the scale of intracellular organelles, close to the primary photosynthetic and respiration events. A direct formulation on biomass concentration is another option (both oxygen and biomass productions being linked by the stoichiometric equation of growth). However, consideration of oxygen offers several advantages: it is well established that for dynamics shorter than several minutes, the resulting net oxygen evolution rate observed at the macroscopic reactor scale (considering a negative respiration volume; see later on in this chapter) cannot be related to an auto-consumption of the biomass itself (from intracellular reserves). This level of representation is also compatible with characteristic times such as mixing or circulation times in the PBR (a minute as an order of magnitude), which could interact with cofactor reduction and re-oxidation on the electron carrier chains, with a coupling at the primary stage of the intracellular metabolism, leading to the light/dark cycle effect (described below). These processes are thus all directly and stoichiometrically linked to oxygen evolution/consumption.

When considering oxygen evolution/consumption, it is useful to introduce the compensation point of photosynthesis G_C (Cornet et al. 1992; Cornet and Dussap 2009; Takache et al. 2010). By definition, irradiance values higher than G_C are necessary for a net positive photosynthetic growth (strictly, a net oxygen evolution rate). Irradiances below the G_C value have different effects depending on whether eukaryotic (microalgae) or prokaryotic (cyanobacteria) cells are considered. As cyanobacteria have their respiration inhibited by light for short residence time, exposure to dark (Myers and Kratz 1955; Gonzalez de la Vara and Gomez-Lojero 1986) and a nil oxygen evolution rate for irradiances below the G_C value can be assumed. For eukaryotic microalgae, photosynthesis and respiration operate separately in chloroplasts and mitochondria. Hence microalgae, unlike cyanobacteria, present respiration both in the dark and in light. Oxygen-consumption rates will thus be obtained for values below G_C.

The kinetic response must be related to the heterogeneous light distribution in cultivation systems. Following the pioneering work of Irazoqui et al. (1976) and Spadoni et al. (1978) on photoreactors, and that of Aiba (1982) on photobioreactors, the authors have extensively developed this coupling formulation from the specific absorbed local radiant light power density $\mathcal{A}$ ($\mu mol_{h\nu}.s^{-1}.kg^{-1}$ or $W.kg_X^{-1}$) as deduced from the local value of irradiance G inside the PBR ($A = \int_{PAR} Ea_\lambda G_\lambda \, d\lambda$). This approach was improved recently by the authors (Cornet and Dussap 2009),

who derived predictive values for the energetic and quantum yields involved in the case of cyanobacteria. As previously explained, regarding the inhibition of respiration by light, the following equation was obtained:

$$J_{O_2} = \rho\,\overline{\varphi}'_{O_2}\mathcal{A}\,\mathcal{H}(G - G_C) = \rho_M \frac{K}{K+G}\overline{\varphi}'_{O_2}\mathcal{A}\,\mathcal{H}(G - G_C) \tag{10.15}$$

where $\mathcal{H}(G - G_C)$ is the Heaviside function ($\mathcal{H}(G - G_C) = 0$ if $G < G_C$ and $\mathcal{H}(G - G_C) = 1$ if $G > G_C$). $\rho = \rho_M \frac{K}{K+G}$ is the energetic yield for photon conversion of maximum value ρ_M (demonstrated to be roughly equal to 0.8), $\overline{\varphi}'_{O_2} = \upsilon_{O_2-X}\overline{\varphi}'_X = \frac{1}{4(1 + P/2e^-)}$ is the molar quantum yield for the *Z*-scheme of photosynthesis (deduced from the structured stoichiometric equations as presented above), and K is the half saturation constant for photosynthesis depending on the microorganism considered.

This formulation was recently completed for the specific case of microalgae with an additional term (right-hand term in Eq. (10.16)) to consider respiration activity in light (Takache *et al.* 2012). This was found to be necessary, especially if a dark zone appears in the culture volume (a very common occurrence when cultivating algae) because of the significant contribution of respiration to the resulting growth in the whole PBR. In the case of microalgae, the following equation was thus proposed:

$$J_{O_2} = \left[\rho\,\overline{\varphi}'_{O_2}A - \frac{J_{NADH_2}}{\upsilon_{NADH_2-O_2}} \times \frac{K_r}{K_r+G}\right] = \left[\rho_M \frac{K}{K+G}\overline{\varphi}'_{O_2}A - \frac{J_{NADH_2}}{\upsilon_{NADH_2-O_2}} \times \frac{K_r}{K_r+G}\right] \tag{10.16}$$

with J_{NADH_2} the specific rate of cofactor regeneration on the respiratory chain, here linked to oxygen consumption by the stoichiometric coefficient $\upsilon_{NADH_2-O_2}$ (the stoichiometric coefficient of cofactor regeneration on the respiratory chain). We note that the effect, well known to physiologists, of the radiation field on the respiratory activity term was taken into account as an adaptive process of the cell energetics (Peltier and Thibault 1985; Cournac et al. 2002; Cogne et al. 2011). The decrease in respiration activity with respect to light was modeled here by an irradiance-dependent relation, by simply introducing in a preliminary approach an inhibition term with a constant K_r describing the decreased respiration in light. We emphasize that this parameter is entirely determined by the knowledge of the irradiance of compensation ($J_{O_2}(G_C) = 0$) when the specific respiration rate J_{NADH_2} is known.

As a direct result of the light distribution inside the culture, the kinetic relation (Eq. (10.15) or Eq. (10.16) for cyanobacteria and microalgae respectively) is of the local type. This implies calculating the corresponding mean value by averaging over the total culture volume V_R:

$$< J_{O_2} > = \frac{1}{V_R} \iiint_{V_R} J_{O_2} \mathrm{d}V \tag{10.17}$$

For a cultivation system with Cartesian one-dimensional light attenuation (see later), this consists of a simple integration along the depth of culture z:

$$< J_{O_2} > = \frac{1}{L} \int_{z=0}^{z=L} J_{O_2} \mathrm{d}z \tag{10.18}$$

in which L is the reactor depth.

We note that in the particular case of cyanobacteria, for which growth can be neglected for values below G_c because of the inhibition of respiration by light (as explained by the Heaviside function in Equation (10.15)), the integrand can be restricted to the illuminated volume V_1 of the cultivation system (values higher than G_C corresponding to the illuminated fraction of the reactor y – see Eq. (10.30)), reducing the integral to:

$$< J_{O_2} > = \frac{1}{V_R} \iiint_{V_1} J_{O_2} \mathrm{d}V \tag{10.19}$$

where V_1 is obtained from the knowledge of the irradiance field in the PBR, enabling us to determine the proportion of the reactor volume in which the irradiance G is higher than the irradiance of compensation G_C.

Finally, once $< J_{O_2} >$ is known, the mean volumetric biomass growth rate $< r_X >$ can be deduced directly using the associated stoichiometry (considering the actual illumination conditions):

$$< r_X > = \frac{< J_{O_2} > C_X M_X}{\upsilon_{O_2 - X}} \tag{10.20}$$

Hence the mass balance equation (Eq. (10.5) or (10.6)) can be solved for any operating conditions of light-limited growth.

10.3.5 Energetics of photobioreactors

The energy analysis of photobioreactors, associated with their previous kinetic study, is also of prime importance, especially if the biomass growth is dedicated to producing an energy vector such as biofuel or hydrogen. This point has prompted intense controversy regarding, for example, the maximal surface productivities that could be achieved with intensive microalgal cultivation, and there is evidently much confusion on this issue in the literature.

However, the rigorous equation giving the thermodynamic efficiency of any PBR from molar kinetic rates $<r_j'>$ is established as follows (Cornet et al. 1994):

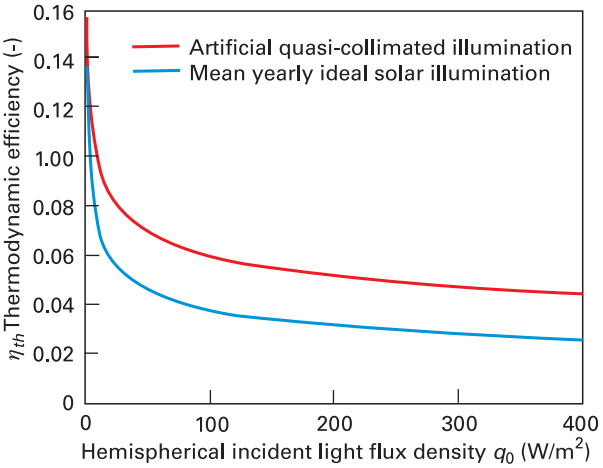

Fig. 10.4: Evolution of the thermodynamic efficiency η_{th} of a rectangular photobioreactor illuminated on one side with a collimated radiation versus the incident PFD q_0. The negative effect of the incident angular dependence θ for the solar illumination (maximum $\overline{\cos\theta} = 0.64$) in comparison with the normal incidence ($\cos\theta = 1$) for artificial illumination is clearly established. The rapid decrease in the PBR efficiency with increasing the incident PFD is also emphasized.

$$\eta_{\mathrm{th}} = \frac{\sum_{j=1}^{r}\sum_{p=1}^{n} \upsilon_{pj} < r'_j > \tilde{\mu}_p}{< \mathrm{A} > - \sum_{j=1}^{r}\sum_{s=1}^{m} \upsilon_{sj} < r'_j > \tilde{\mu}_s} \tag{10.21}$$

in which the $\tilde{\mu}_{p,s}$ are respectively the chemical potentials for products and substrates involved in the jth reaction and $<\mathcal{A}>$ the mean averaged volumetric radiant power density absorbed in the PBR (derived from the knowledge of the radiation field – see later on in this chapter). In a first approximation, the chemical potential may be substituted by standard Gibbs free enthalpies $\Delta g_i'^{0}$ for the products and substrates (Roels 1983) which enables us to use this equation, combined with the previous kinetic models for the assessment of the molar rates $<r'_j>$. On the other hand, we can envisage a direct calculation of the same thermodynamic efficiency η_{th} from knowledge models describing the energy conversion at each stage of the cell metabolism from primary photosynthetic events to total biomass synthesis (a dynamic analysis encompassing 15 orders of magnitude for characteristic time constants!). This work is currently being undertaken by the authors using the linear energy converters theory (Cornet *et al.* 1998), enabling us to derive general results for the efficiency of photosynthesis via microalgal cultivation in PBR (Cornet 2007).

As an example, Figure 10.4 shows the results obtained for a microorganism cultivated on ammonia as N-source (such as *C. reinhardtii*) in a rectangular PBR

artificially illuminated on one side with a quasi-collimated PFD, and the same PBR in ideal solar conditions (Pruvost et al. 2012) (only direct illumination with a mean maximum $\overline{\cos\theta}$ = 0.64 – see later for explanations). The same calculations with nitrate as N-source (*A. platensis*, for example) would lead to the same evolution with 20 % lower efficiencies. These results have been shown to agree closely with experimental results obtained on different sizes of PBR (Cornet 2010).

These results clearly demonstrate the marked decrease in PBR efficiency with increasing PFD because of different factors of dissipation mainly affecting the functioning of the Z-scheme in the photosynthesis. As the authors have clearly established that the surface productivity of a solar PBR is proportional to its thermodynamic efficiency, they recently proposed (Cornet 2010) the concept of dilution of the incident radiation to improve the performance of outdoor solar PBRs. It is possible (see Fig. 10.4), instead of working at an efficiency of 2–3 % with direct solar capture, to operate by capture/dilution at very low incident PFD with efficiencies of around 15 % (and with a very high specific illuminated area) as proposed in the DiCoFluV concept (Cornet 2010).

Figure 10.4 also emphasizes the negative effect of the time-varying collimated incidence in solar illumination (see Fig. 10.2) in comparison with a continuous normal incidence on an artificially illuminated PBR. This effect has recently been analyzed (Pruvost *et al.* 2012) as a consequence of a different averaged field of radiation inside the reactor for the two situations, demonstrating once again the need for a proper description of the local radiation field inside the culture volume.

Finally, these theoretical results, associated with Equation (10.21) and with ideal solar data for earth surface illumination, allow a rigorous calculation of the yearly maximum performances of solar PBR in optimal running conditions (hypothetical location at the Equator with maximum yearly ground illumination and ammonium as N-source) as a thermodynamic limit for photosynthesis engineering. The values obtained were respectively 50 $t_X.ha^{-1}.yr^{-1}$ for a fixed PBR with direct sunlight capture and 400 $t_X.ha^{-1}.yr^{-1}$ for a PBR with optimal light dilution and a tracking capture system (Cornet 2010). As explained above, these values are 20 % lower when nitrate is the N-source, giving 40 $t_X.ha^{-1}.yr^{-1}$ for a direct capture system and 320 $t_X.ha^{-1}.yr^{-1}$ for a dilution system.

10.3.6 Radiative transfer modeling

The above energy and kinetic models emphasize the crucial importance of radiative transfer modeling as the only way to access local information in turbid cultivation media with confidence. This radiative transfer modeling may be performed from many different approaches depending on the final accuracy and robustness sought for the growth model (Yun and Park 2003). As regards empirical models for formu-

lating the coupling between light and kinetics, there is no need to develop a rigorous description of the radiative transfer inside the culture bulk. In this case, although it holds only in a given direction (i.e. in intensity and not in flux density of irradiance, as often incorrectly assumed in the literature) and although it does not account for scattering by cells, the Lambert–Beer law (strictly, Bouguer's law) can be applied to obtain a tendency and sometimes to calculate any mean averaged illumination quantity on the PBR. For the authors, who have spent a long time developing predictive knowledge models of PBRs, it is clear, by contrast, that a fine formulation of the kinetic coupling requires first knowledge of the local irradiance at any point of the culture bulk, and in this case the use of the rigorous radiative transfer equation (RTE) solutions is then necessary. The field of irradiance obtained in this way enables us to calculate the local volumetric radiative power density absorbed (see Section 10.3.4), which is the key variable needed to formulate both the energy coupling (Cornet *et al.* 1994, Cornet 2005) and the kinetic coupling, as is known from the pioneering work of Irazoqui et al. (1976) popularized by the team of Cassano and Alfano (Cassano *et al.* 1995) on photoreactors and used for the first time in PBR modeling by Aiba (1982).

10.3.6.1 Radiative transfer equation

The radiative transfer equation or RTE (a linear Boltzmann-type integro-differential equation) was originally developed by Chandrasekhar (1960). It takes into account the scattering of light by the micro-organisms considered as scatterers, and enables us (if the incident PFD is known accurately enough) to calculate with accuracy and confidence the spectral field of irradiance inside the culture medium, once the angular integration over the intensities has been performed (see Part 2.1). From the notations adopted in this chapter, it takes the following form for direction $\mathbf{\Omega}$ and wavelength λ:

$$(\mathbf{\Omega} \cdot \nabla) I_\lambda (\mathbf{r}, \mathbf{\Omega}, t) = -(a_\lambda + s_\lambda) I_\lambda (\mathbf{r}, \mathbf{\Omega}, t) + \frac{s_\lambda}{4\pi} \iint_{4\pi} I_\lambda (\mathbf{r}, \mathbf{\Omega}', t) p_\lambda (\mathbf{\Omega}, \mathbf{\Omega}') \, \mathrm{d}\Omega' \tag{10.22}$$

where a_λ, s_λ and $p_\lambda (\Omega, \Omega')$ are the volumetric absorption and scattering coefficients with the phase function (the radiative properties – see later on in this chapter), requiring us to define a five-dimensional Euclidean frame of reference as presented in Figure 10.5.

Finding a general three-dimensional solution to this equation (once the radiative properties of the micro-organisms are known – see later on in this chapter) using the appropriate form of the transport operator (see Tab. 10.1) is generally a difficult problem. There are deterministic numerical methods such as finite element methods (Cornet *et al.* 1994) and finite volume methods (Siegel and Howell

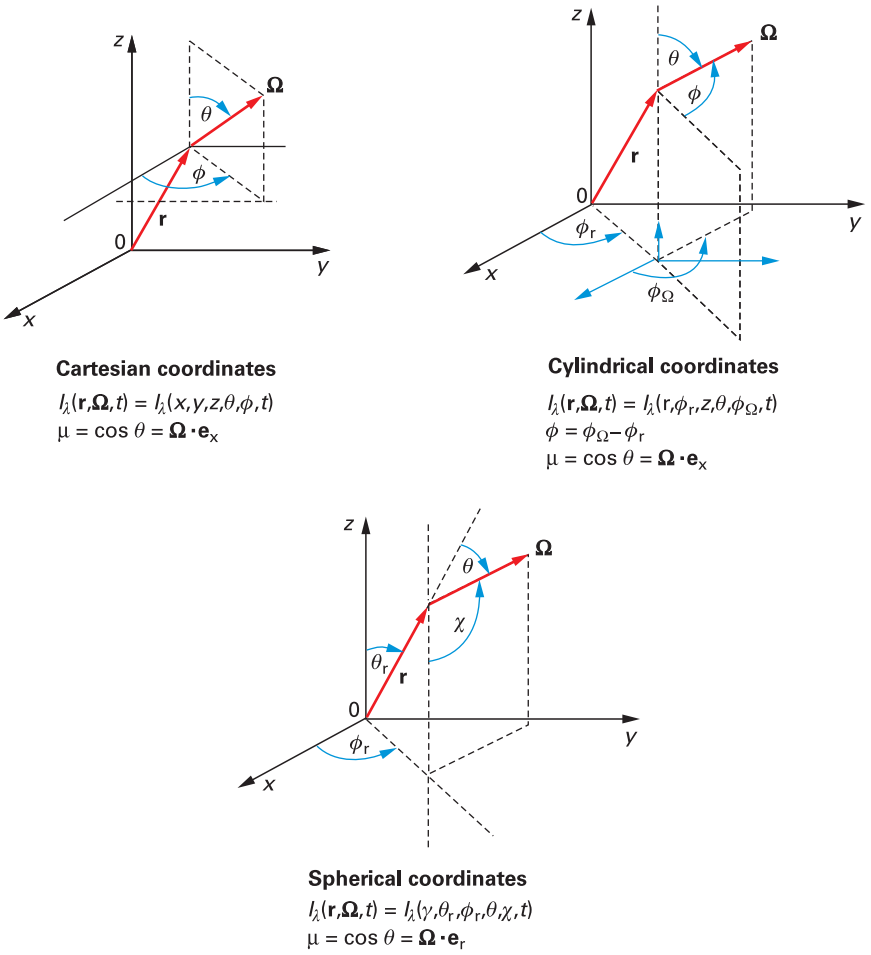

Fig. 10.5: Definitions of fixed and moving frames of reference in different coordinate systems for the ETR.

2002), or stochastic numerical methods such as direct Monte Carlo methods (Aiba 1982; Csogör *et al.* 2001) and integral Monte Carlo methods (Dauchet *et al.* 2012a). Fortunately, for many practical situations, it is possible to reduce the above problem to a more simple treatment of the RTE involving a one-dimensional approximation. In this case, the RTE reduces to (for any coordinate axis $u = z$ or r and defining systematically, in contrast to Figure 10.5 for curvilinear coordinates systems, the angle β between the axis u and the corresponding direction of I_λ):

$$\cos\beta\frac{\mathrm{d}I_\lambda(u,\beta,t)}{\mathrm{d}u} = -(a_\lambda + s_\lambda)I_\lambda(u,\beta,t) + \frac{s_\lambda}{2}\int_0^\pi I_\lambda(u,\beta',t)\,p_\lambda(\beta,\beta')\sin\beta'\,\mathrm{d}\beta' \quad (10.23)$$

This simpler integro-differential equation may be solved, for example, by the differential discrete ordinates method (DOM) as proposed for turbid water media by Houf and Incropera (1980) and improved by Kumar *et al.* (1990), but achieving the required accuracy then requires long calculation times if classical solvers of boundary value problems are used (Mattheij and Staarink 1984a, 1984b; Kumar *et al.* 1990). The authors have recently implemented a matrix method using Matlab® software, and this has proven to be very much faster than the other Fortran or C routines hitherto available. In this case, the one-dimensional ETR (Eq. (10.23)) is transformed into a differential system of N equations corresponding to the cosine directions ($N \times N$ diagonal matrix $\mathbf{M}$ for cos β_i) and the weights ($N \times N$ diagonal matrix $\mathbf{W}$) of a Lobatto quadrature. This leads to the following system in matrix notation, and in Cartesian coordinates:

$$\frac{\mathrm{d}\mathbf{i}}{\mathrm{d}\tau_\lambda} = \frac{\mathbf{M}^{-1}}{N}\left[(N-1)\left(-\mathbf{D} + \frac{\varpi_\lambda}{2}\mathbf{PW}\right)\mathbf{i} - (1-\varpi_\lambda)\,\mathbf{i}\right] \tag{10.24}$$

in which $\mathbf{D} = \delta_{ij}$ is the Kronecker delta, $\mathbf{i}$ is the vector of intensities, $\mathbf{P}$ is an $N \times N$ matrix for the phase function calculation, $\varpi_\lambda = s_\lambda / (a_\lambda + s_\lambda)$ is the albedo of single scattering, and $\tau_\lambda = (a_\lambda + s_\lambda)\,u$ is the optical thickness.

Lastly, a final simplification consists in retaining only two ordinates in Equation (10.24) and averaging the intensities over each positive and negative hemisphere, providing a hypothesis for its angular dependence in the medium considered. This is the well-known two-flux method originally developed in Cartesian coordinates by Schuster (1905) with the diffuse hypothesis and by Hottel and Sarofim (1967) for the collimated hypothesis: it was improved by the authors in the 2000s to allow work in any geometry and for any angular distribution of the intensities (Takache et al. 2010). The main advantage of this simple method is that it leads, in many practical cases of interest, to analytical solutions (if the lack of accuracy is accepted) for the calculation of the field of radiation. For the example of a slab irradiated from one side with a reflectivity ρ_λ at the rear (corresponding, for example, to a flat panel PBR with reflecting rear side as obtained with stainless steel), we obtain (Cornet et al. 1995; Pottier *et al.* 2005; Farges *et al.* 2009) for the spectral irradiance G_λ (and for the simpler special case of a nonreflecting back side, *i.e.* $\rho_\lambda = 0$):

$$\frac{G_\lambda}{q_{o,\lambda}} = K\frac{[\rho_\lambda(1+\alpha_\lambda)\exp(-\delta_\lambda L) - (1-\alpha_\lambda)\exp(-\delta_\lambda L)]\exp[\delta_\lambda z] + [(1+\alpha_\lambda)\exp(\delta_\lambda L) - \rho_\lambda(1-\alpha_\lambda)\exp(\delta_\lambda L)]\exp[-\delta_\lambda z]}{(1+\alpha_\lambda)^2\exp(\delta_\lambda L) - (1-\alpha_\lambda)^2\exp(-\delta_\lambda L) + \rho_\lambda(1-\alpha_\lambda)^2[\exp(-\delta_\lambda L) - \exp(\delta_\lambda L)]}$$

$$\frac{G_\lambda}{q_{o,\lambda}} = K\frac{[(1+\alpha_\lambda)\exp[-\delta_\lambda(z-L)]] - [(1-\alpha_\lambda)\exp[\delta_\lambda(z-L)]]}{(1+\alpha_\lambda)^2\exp(\delta_\lambda L) - (1-\alpha_\lambda)^2\exp(-\delta_\lambda L)} \quad \text{if } \rho_\lambda = 0 \tag{10.25}$$

in which n is the degree of collimation ($n = 0$ for isotropic intensities and $n = \infty$ for collimated intensity in direction β_c), and:

$$K = 2\left(\frac{n+2}{n+1}\right)\sec\beta_c$$

$$\alpha_\lambda = \sqrt{\frac{a_\lambda}{(a_\lambda + 2b_\lambda s_\lambda)}} \qquad \delta_\lambda = \sec\beta_c\left(\frac{n+2}{n+1}\right)\sqrt{a_\lambda\,(a_\lambda + 2\,b_\lambda s_\lambda)}$$

and the backscattered fraction

$$b_\lambda = \frac{1}{2}\int_{\pi/2}^{\pi} p_\lambda\,(\beta\,,\,\beta')\sin\beta\,\mathrm{d}\beta$$

Likewise, the method can be used for a cylindrical PBR (Cornet 2010; Takache *et al.* 2010) leading, for example, in the case of a radial illumination with the same notations and considerations, to:

$$\frac{G_\lambda}{q_{R,\lambda}} = 2\left(\frac{n+2}{n+1}\right)\frac{\mathrm{I_0}(\delta_\lambda r)}{(1-\rho_\lambda)\,\mathrm{I_0}(\delta_\lambda R) + \alpha_\lambda(1+\rho_\lambda)\,\mathrm{I_1}(\delta_\lambda R)}$$

$$\frac{G_\lambda}{q_{R,\lambda}} = 2\left(\frac{n+2}{n+1}\right)\frac{\mathrm{I_0}(\delta_\lambda r)}{\mathrm{I_0}(\delta_\lambda R) + \alpha_\lambda\,\mathrm{I_1}(\delta_\lambda R)} \text{ if } \rho_\lambda = 0 \tag{10.26}$$

where the $I_n(x)$ are the n order modified Bessel functions of first species.

The accuracy of the useful two-flux approximation is nevertheless not always satisfactory and depends mainly on the information required. The comparison between the rigorous differential discrete ordinates method (with $N = 32$, Eq. (10.24)) and the two-flux approximation (Eq. (10.25)) with the example of radiative properties of *A. platensis* at 540 nm is shown in Figure 10.6. As already discussed from a comparison with experimental data for other micro-organisms (Pottier et al. 2005), the two-flux approximation is rather good so long as $G/q_0 > 0.1$ and in the special case of quasi-collimated incidence, a situation in close agreement with the forward scattering behavior of micro-organisms as scatterers. This assumption may thus be used in this case as a good approximation unless local information with low irradiance values is sought, such as irradiance of compensation G_C. In this case, a more accurate method (e.g. DOM or Monte Carlo), as presented in this chapter, is needed.

The two-flux approximation may also be useful for modeling light transfer in solar PBRs requiring us first to separate the collimated (direct) and diffuse (isotropic) contributions at any given time and second to solve the light transfer with dynamic variations in the angular pattern and intensity of the PFD, requiring longer computation time. This work was recently carried out by the authors to obtain full yearly simulations of rectangular PBRs installed at different terrestrial

Cartesian coordinates:

$$(\Omega \cdot \nabla)\,\Psi = \left(1-\mu^2\right)^{1/2}\left[\cos\varphi\frac{\partial\Psi}{\partial x} + \sin\varphi\frac{\partial\Psi}{\partial y}\right] + \mu\frac{\partial\Psi}{\partial z}$$

$$= \sin\theta\cos\varphi\frac{\partial\Psi}{\partial x} + \sin\theta\sin\varphi\frac{\partial\Psi}{\partial y} + \cos\theta\frac{\partial\Psi}{\partial z}$$

$$q_{\lambda,x} = \int_0^{2\pi}\int_0^{\pi} I_\lambda\cos\varphi\sin^2\theta\,\mathrm{d}\theta\,\mathrm{d}\varphi\,,\; q_{\lambda,y} = \int_0^{2\pi}\int_0^{\pi} I_\lambda\sin\varphi\sin^2\theta\,\mathrm{d}\theta\,\mathrm{d}\varphi\,,\; q_{\lambda,z} = \int_0^{2\pi}\int_0^{\pi} I_\lambda\cos\theta\sin\theta\,\mathrm{d}\theta\,\mathrm{d}\varphi$$

$$= \int_0^{2\pi}\int_{-1}^{1} I_\lambda\,\mu\,\mathrm{d}\mu\,\mathrm{d}\varphi$$

Cylindrical coordinates:

$$(\Omega \cdot \nabla)\,\Psi = (1-\mu^2)^{1/2}\cos\varphi\frac{\partial\Psi}{\partial r} + \frac{(1-\mu^2)^{1/2}}{r}\sin\varphi\left[\frac{\partial\Psi}{\partial\varphi_r} - \frac{\partial\Psi}{\partial\varphi}\right] + \mu\frac{\partial\Psi}{\partial z}$$

$$= \sin\theta\cos\varphi\frac{\partial\Psi}{\partial r} + \frac{\sin\theta\sin\varphi}{r}\left[\frac{\partial\Psi}{\partial\varphi_r} - \frac{\partial\Psi}{\partial\varphi}\right] + \cos\theta\frac{\partial\Psi}{\partial z}$$

$$q_{\lambda,r} = \int_0^{2\pi}\int_0^{\pi} I_\lambda\cos\varphi\sin^2\theta\,\mathrm{d}\theta\,\mathrm{d}\varphi\,,\; q_{\lambda,\varphi} = \int_0^{2\pi}\int_0^{\pi} I_\lambda\sin\varphi\sin^2\theta\,\mathrm{d}\theta\,\mathrm{d}\varphi\,,\; q_{\lambda,z} = \int_0^{2\pi}\int_0^{\pi} I_\lambda\cos\theta\sin\theta\,\mathrm{d}\theta\,\mathrm{d}\varphi$$

$$= \int_0^{2\pi}\int_{-1}^{1} I_\lambda\,\mu\,\mathrm{d}\mu\,\mathrm{d}\varphi$$

Spherical coordinates:

$$(\boldsymbol{\Omega} \cdot \nabla)\;\Psi = \mu\frac{\partial\Psi}{\partial r} + \frac{(1-\mu^2)^{1/2}}{r}\frac{\sin\chi}{\sin\theta_r}\frac{\partial\Psi}{\partial\varphi_r} + \frac{(1-\mu^2)^{1/2}}{r}\cos\chi\frac{\partial\Psi}{\partial\theta_r} + \frac{1-\mu^2}{r}\frac{\partial\Psi}{\partial\mu} - \frac{(1-\mu^2)^{1/2}}{r}\frac{\sin\chi}{\tan\theta_r}\frac{\partial\Psi}{\partial\chi}$$

$$= \cos\theta\frac{\partial\Psi}{\partial r} + \frac{\cos\theta}{r}\frac{\sin\chi}{\sin\theta_r}\frac{\partial\Psi}{\partial\varphi_r} + \frac{\cos\theta}{r}\cos\chi\frac{\partial\Psi}{\partial\theta_r} - \frac{\sin\theta}{r}\frac{\partial\Psi}{\partial\theta} - \frac{\cos\theta}{r}\frac{\sin\chi}{\tan\theta_r}\frac{\partial\Psi}{\partial\chi}$$

$$q_{\lambda,r} = 2\pi\int_0^{\pi} I_\lambda\cos\theta\sin\theta\,\mathrm{d}\theta \;=\; 2\pi\int_{-1}^{1} I_\lambda\,\mu\,\mathrm{d}\mu$$

Tab. 10.1: Definitions of the operator of transport $(\boldsymbol{\Omega} \cdot \nabla)$ and of the radiant light flux density q in different systems of coordinates as defined in Figure 10.5

locations (Pruvost *et al.* 2012). The incident PFD q is thus divided into the direct $q_{//}$ (θ angle-dependent; see Fig. 10.2) and the isotropic diffuse $q_{\cap}$ parts ($q = q_{//} + q_{\cap}$) respectively. The general analytical solution can be easily obtained

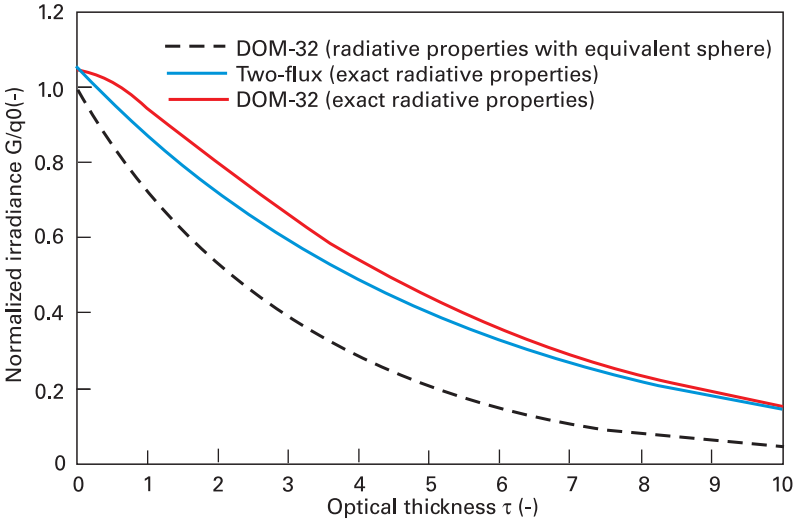

Fig. 10.6: Comparison between a rigorous differential discrete ordinates method with $N = 32$ (DOM-32, Eq. (10.24)) and the two-flux approximation (Eq. (10.25)) for a rectangular PBR illuminated on one side with a quasi-collimated incident PFD and with the radiative properties of *A. platensis* at 540 nm. The effect of approximating the quasi-exact radiative properties by equivalent spheres using the Lorenz–Mie theory is also reported.

from Equation (10.25), neglecting here the reflectivity at the rear surface ($\rho = 0$) and using mean spectral averaged radiative properties for simplicity. Taking the degree of collimation $n = 0$ ($\beta_c = \theta = 0$) for diffuse radiation and $n = \infty$ ($\beta_c = \theta$ a function of time) for direct radiation then gives the two analytical fields of irradiance:

$$\frac{G_{\mathrm{col}}}{q_{//}} = \frac{2}{\cos\theta} \frac{(1+\alpha)\exp[-\delta_{\mathrm{col}}(z-L)] - (1-\alpha)\exp[\delta_{\mathrm{col}}(z-L)]}{(1+\alpha)^2\exp[\delta_{\mathrm{col}}L] - (1-\alpha)^2\exp[-\delta_{\mathrm{col}}L]} \tag{10.27}$$

$$\frac{G_{\mathrm{dif}}}{q_{\cap}} = 4\frac{(1+\alpha)\exp[-\delta_{\mathrm{dif}}(z-L)] - (1-\alpha)\exp[\delta_{\mathrm{dif}}(z-L)]}{(1+\alpha)^2\exp[\delta_{\mathrm{dif}}L] - (1-\alpha)^2\exp[-\delta_{\mathrm{dif}}L]} \tag{10.28}$$

with:

$$\delta_{\mathrm{col}} = \frac{\sqrt{a(a+2bs)}}{\cos\theta} \qquad \delta_{\mathrm{dif}} = 2\sqrt{a(a+2bs)}$$

The total irradiance (representing the amount of light impinging on algae) is finally given by simply summing the collimated and diffuse components:

$$G(z) = G_{\text{col}}(z) + G_{\text{dif}}(z) \tag{10.29}$$

Equations (10.27) and (10.28) show that penetrations of collimated and diffuse radiations inside the culture volume are markedly different (Pruvost et al. 2012). This will be especially important in solar conditions where the diffuse component of the radiation is non-negligible. We also note the influence of the incident angle θ on the collimated part, light penetration decreasing with increasing incident angle. Like the degree of collimation of the radiation, this will influence cultivation system efficiency (for a more detailed description, see Pruvost *et al.* 2012).

10.3.6.2 Optical and radiative properties for micro-organisms

As explained above, a sound description of the radiant light transfer in the culture volume of the PBR is necessary if knowledge-based kinetic and energy coupling formulations are envisaged in the modeling approach. In this case, it is emphasized that the radiative properties that appear as parameters in the RTE have to be accurately determined beforehand. If this task is not performed with sufficient care, rigorously solving the RTE will be of little use, and an empirical kinetic model will be preferable. This point is clearly illustrated in Figure 10.6, which compares irradiance profiles calculated for *A. platensis* turbid media with quasi-exact radiative properties (*A. platensis* is then considered as a randomly oriented long circular cylinder) and approximated radiative properties by equivalent spheres, then evidencing a marked discrepancy. These radiative properties are the volumetric absorption $a_\lambda = Ea_\lambda.C_X$ and scattering $s_\lambda = Es_\lambda.C_X$ coefficients (Ea_λ and Es_λ being the mass absorption and scattering coefficients for the biomass concentration C_X) and the phase function for scattering $p_\lambda(\mathbf{\Omega}, \mathbf{\Omega}')$, all appearing in the RTE (Eq. (10.22)). They physically represent the probability of a photon being absorbed by the cell or scattered in a given direction, and can be deduced theoretically from the absorption and scattering cross-sections of the micro-organisms. The assessment of these radiative properties for all the wavelengths in the PAR (we have demonstrated in fact that roughly 50 values over the PAR range afford sufficient accuracy in most cases) is generally a difficult task. It can be tackled either experimentally or theoretically.

The experimental determination of the absorption and scattering coefficients requires working with an integrating sphere to measure transmittance or reflectance of the samples, the single scattering condition simplifying the inversion procedure. The determination of the angular phase function for scattering is far more difficult and requires a nephelometer (the laser of which generally works only at a given set of wavelengths). This wide and important experimental field has been extensively explored and developed during the last 10 years by Pilon and Berberoglu (Berberoglu and Pilon 2007; Pilon et al. 2011). If the inversion is performed from transmittance or reflectance results obtained in multiple scattering conditions, it

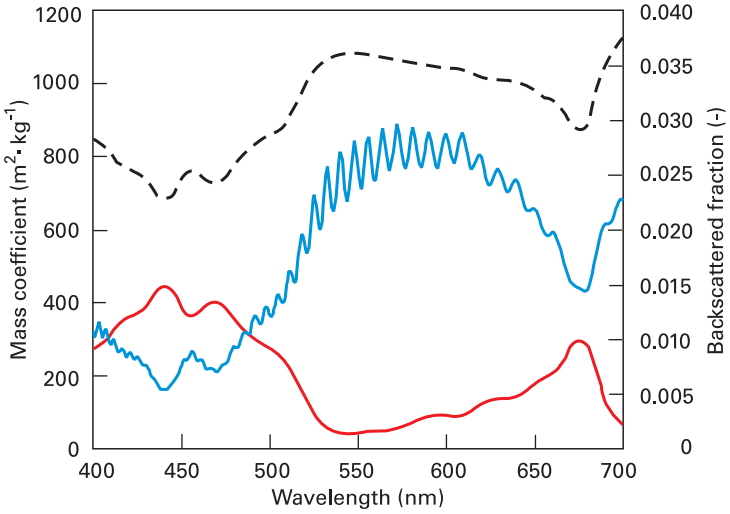

Fig. 10.7: Example of the calculation of radiative properties for the microalga *Chlamydomonas reinhardtii* calculated from optical properties as defined by Pottier et al. (2005) and using the equivalent sphere approximation (log-normal size distribution) with the Lorenz–Mie theory. Bold solid line: mass absorption coefficient *E*a; dashed line: mass scattering coefficient *E*s; thin solid line: backscattered fraction.

is necessary to guarantee an exact RTE solution using, for example, a zero-variance integral Monte Carlo method (Dauchet *et al.* 2012a).

One limitation of the experimental approach is its lack of predictability, as radiative properties vary with the cultivation conditions (CO_2 or mineral limitations, PFD, etc.), which has marked effects on the pigment contents or the size distribution of the cells. It is then possible to calculate radiative properties using a purely theoretical approach by solving the Maxwell equations of electromagnetism around the particles in spherical coordinates (Mishchenko et al. 2000). Solving this problem using a model of equivalent sphere for the micro-organisms is referred to as the Lorenz–Mie theory, which today is quite easy to compute (Bohren and Huffman 1983; Pottier *et al.* 2005). As this approximation has been shown to be of low accuracy for the numerous different shapes encountered in the world of microalgae (see Fig. 10.6), often very different from spheres, the authors are currently developing a predictive method (Dauchet *et al.* 2012b) that allows radiative properties to be computed for any given shape of rotationally symmetric randomly oriented scatterers from the anomalous diffraction approximation (Van de Hulst 1981). The input parameters are merely the pigment contents and the size distributions of the cells, the former enabling us to calculate the imaginary part of the refractive index for the particles from "*in vivo*" databases (Bidigare *et al.* 1990), as previously explained elsewhere (Pottier *et al.* 2005). The real parts of the refractive indices are then computed according to the Kramers–Kronig relations (Lucarini et

al. 2005). For microalgae with quasi-spherical shapes, the sphere-equivalent model may nevertheless be a good first approximation for the calculation of radiative properties. For example, Figure 10.7 illustrates results obtained by the proposed approach for *C. reinhardtii*, using the method of Pottier et al. (2005) for assessment of optical properties, and the Lorenz–Mie theory of equivalent spheres (Bohren and Huffman 1983) for the calculation of the radiative properties (here summarized as spectral absorption and scattering mass coefficients Ea_λ, Es_λ and spectral back-scattered fraction b_λ).

10.4 Illustrations of the utility of modeling for the understanding and optimization of cultivation systems

10.4.1 Understanding the role of light-attenuation conditions

10.4.1.1 Illuminated fraction *y*

Illumination conditions (as represented by the incident PFD) are a major operating parameter of any cultivation system. Their influence is, however, difficult to process. This is because of their relation to light-attenuation conditions in the culture volume, which in turn affect photosynthetic conversion and thereby the overall cultivation system. Modeling light-transfer conditions using adequate radiative transfer models as described above is in this regard of primary importance. A specific, easy-to-use parameter, named "illuminated volume fraction" and noted y, has been found to be especially useful. This parameter is directly deduced by the irradiance distribution as obtained from the radiative transfer model (Cornet et al. 1992; Cornet and Dussap 2009; Degrenne et al. 2010; Takache et al. 2010). Schematically, the culture bulk can be delimited into two zones, an illuminated zone and a dark zone (Fig. 10.8). Partitioning is obtained by the compensation irradiance value G_C corresponding to the minimum value of radiant energy required to obtain a positive photosynthetic growth rate. For example, compensation irradiances $G_C = 1.5\ \mu mole.m^{-2}.s^{-1}$ (Cornet and Dussap 2009) and $G_C = 10\ \mu mole.m^{-2}.s^{-1}$ (Takache et al. 2010) were found for *A. platensis* and *C. reinhardtii* respectively. The illuminated fraction y is then given by the depth of the culture z_c where the irradiance of compensation $G(z_c) = G_C$ is obtained (Fig. 10.3). In the case of cultivation systems with one-dimensional light attenuation, we have, for example:

$$y = \frac{V_1}{V_R} = \frac{z_c}{L} \tag{10.30}$$

The y parameter allows three typical cases of light-attenuation conditions to be represented for a given PFD (Fig. 10.8). If the biomass concentration is too low (Case C), part of the incident light is transmitted through the culture and lost for the photoreaction processes. Conversely, if the biomass is too high (Case A), a dark

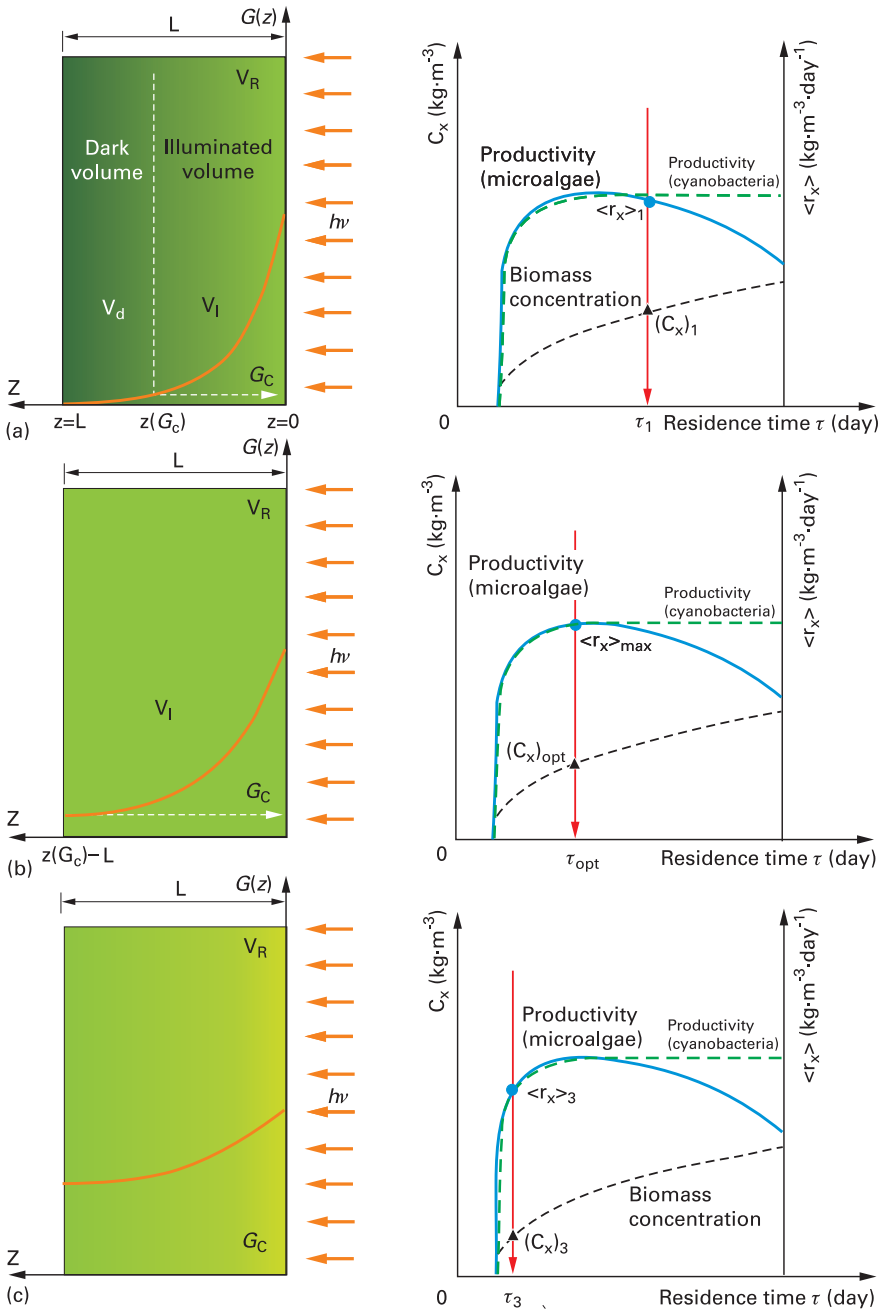

Fig. 10.8: Relation between the light absorption conditions (represented by the irradiance field $G(z)$) and corresponding mean biomass volumetric productivities ($\langle r_x \rangle$). The three typical cases of light-attenuation conditions are represented: full light absorption (Case A), luminostat (Case B) and kinetic regimes (Case C).

zone appears deep in the culture. The former case C with low light absorption is named the "kinetic" regime and is represented by the hypothetical condition "$y > 1$" ($z_c > L$, in this case, the length z_c appears rather as an extinction length, which would require a greater thickness L of the PBR to absorb all the incident radiation). The last case A with full light absorption is represented by the condition "$y < 1$" and corresponds to a light-limited culture. A third typical case can arise: full absorption of the light received, but with no dark zone in the culture volume. This meets the exact condition $y = 1$, also named the "luminostat" regime (Case B, a particular limit case of light-limited culture), and will be demonstrated later as the best condition for optimal productivity (i.e. growth rate) in the PBR.

10.4.1.2 Achieving maximal productivities with appropriate definition of light-attenuation conditions

The growth of photosynthetic microorganisms depends on various parameters. If these can be kept optimal (appropriate regulation of temperature and pH, adequate medium composition), light-limited conditions where light alone limits growth will be achieved. This will, however, be insufficient to guarantee maximal performance of any given cultivation systems (in terms of biomass production of a given species). As shown in Figure 10.8, this requires appropriate light-attenuation conditions to be applied as represented by the illuminated fraction y (Cornet and Dussap 2009; Takache et al. 2010). Because it does not allow full absorption of the light captured, the kinetic regime always leads to a loss of efficiency ($y > 1$). Full light absorption is thus to be preferred ($y \leq 1$). A distinction must be made here between eukaryotic (microalgae) and prokaryotic (cyanobacteria) cells. In the case of cyanobacteria, which have no (or negligible) respiration during short time exposure in the dark (Gonzalez de la Vara and Gomez-Lojero 1986), a dark zone will have no (or little) influence. Meeting the condition $y \leq 1$ will thus be sufficient to guarantee maximal productivity. For eukaryotic cells presenting respiration in the light (microalgae), a dark zone in the culture volume where respiration is predominant will result in a loss of productivity due to reducing power consumption, thus lowering the kinetic rates. Maximal productivity will then require working in the "luminostat" regime with the y fraction meeting the exact condition $y = 1$. These theoretical conditions have been proved experimentally for both cyanobacteria (Cornet and Dussap 2009; Cornet 2010) and microalgae (Takache et al. 2010). Obviously, the determination of light-attenuation conditions by radiative transfer modeling was found in this regard to be most useful for finding the optimal biomass concentration to apply in the cultivation system; see Cornet and Dussap (2009), Cornet (2010) and Takache et al. (2010) for details.

10.4.1.3 Prediction of biomass concentration and productivity

Solving the mass balance equation (Eq. (10.5)) gives biomass concentration C_x for the simulated operating conditions (PBR geometry, PFD, etc.) and for a given spe-

cies (characterized by its radiative properties and kinetic growth parameters). This equation is linked here to an appropriate formulation of kinetic growth (Eq. (10.20), linked to Equation (10.15) or Equation (10.16) for cyanobacteria and microalgae, respectively, here in light-limited conditions) and to radiative transfer conditions in the culture bulk (Eq. (10.25), (10.26), (10.27) or (10.28), depending on the case). Once the biomass concentration is obtained, biomass productivity can be deduced in terms of volumetric ($<r_X>$, $kg.m^{-3}.h^{-1}$) or surface productivity ($<s_X>$, $kg.m^{-2}.h^{-1}$) with the illuminated surface as reference. Volumetric and surface productivities are linked by the following relation:

$$< s_X > = \frac{< r_X > V_R}{S_{light}} = \frac{< r_X >}{a_{light}} \tag{10.31}$$

This equation introduces the specific illuminated surface a_{light}, which represents the ratio of illuminated surface (S_{light}) to volume (V_R) in the cultivation system. We also note that the performance of a cultivation system (in light-limited conditions) when expressed on a surface basis is independent of the cultivation system design (Cornet 2010; Pruvost et al. 2011b).

Figure 10.9 presents results for batch conditions, given here as a first illustration. The illuminated fraction is also represented to emphasize the relation between light-attenuation conditions and resulting productivity. All results are given here for a constant PFD, assuming no limitation other than light. Thus, the time course of growth rate ($<r_x>$) is explained here only by the changes in light conditions in the culture volume due to biomass growth (no nutrient limitation).

Because of their difference in photosynthetic response, microalgae and cyanobacteria present different growth curves. In both cases, the kinetic regime ($y > 1$), usually encountered at the beginning of a batch production run, leads to a loss of efficiency, as illustrated here by a growth rate $<r_x>$ below maximum $<r_{xmax}>$ (values in batch mode are given by the slope of $C_x(t)$; see Eq. (10.5)). This is explained by light transmission, which prevents the full exploitation of the light energy received. Due to the increase in biomass, the y value will decrease progressively to a value below 1. For prokaryotic cells (Fig. 10.9, left), as soon as full absorption is reached, the maximum value of the mean volumetric growth rate will be achieved and then remain constant (until a large dark zone is formed, inducing a shift in the cell metabolism, not represented here). For eukaryotic cells, the $y = 1$ condition, giving the maximum value of the mean volumetric growth rate, will be only transiently satisfied. The increase in the dark volume will then progressively lower the mean volumetric growth rate (Fig. 10.9, right).

The same model can be applied to simulate continuous cultivation (by applying only the appropriate formulation of the mass balance equation, i.e. $\tau \neq 0$ in Eq. (10.5)). In this case, a steady state is obtained for each set of operating conditions with constant biomass concentration and thus constant light-attenuation conditions. An example of the results is given in Figure 10.10 for *C. reinhardtii* growth.

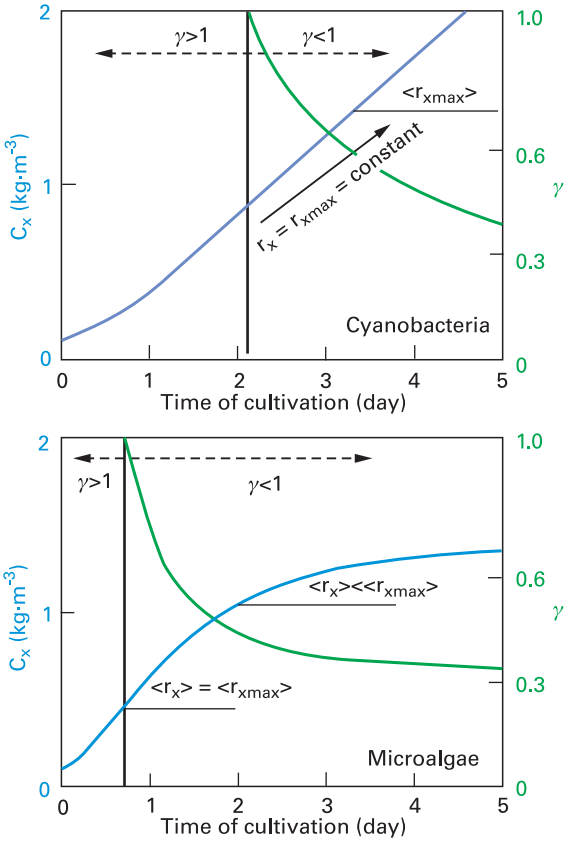

Fig. 10.9: Time course of biomass concentration during a batch cultivation of *Arthrospira platensis* (cyanobacteria, left) and *Chlamydomonas reinhardtii* (microalgae, right) (light-limited conditions). Light attenuation increases with biomass concentration, directly affecting growth kinetics (slope of the curve). This proves to depend entirely on the illuminated fraction γ. We note that due to their respiration activity, microalgae are affected negatively by the formation and expansion of the dark zone ($\gamma < 1$).

The model was found to be accurate over the wide range of PFD investigated (up to 1000 $\mu mol.m^{-2}.s^{-1}$), and for any light-attenuation conditions as obtained by varying the residence time τ and thus biomass concentration. Results are given here for the luminostat regime with $y = 1$ giving maximum biomass productivity, and for full-light absorption with $y = 0.5$. Accurate predictions were also obtained in kinetic regime $y > 1$; see Takache et al. (2012).

Another example is given to illustrate the utility of modeling in PBR engineering. Figure 10.11 presents the results obtained here with the green microalga *Neochloris oleoabundans* cultivated in different PBRs (volume, culture depth) and operating conditions (PFD, residence time). The effects of all of these parameters were accurately predicted. Modeling thus emerges as a highly valuable tool in PBR engi-

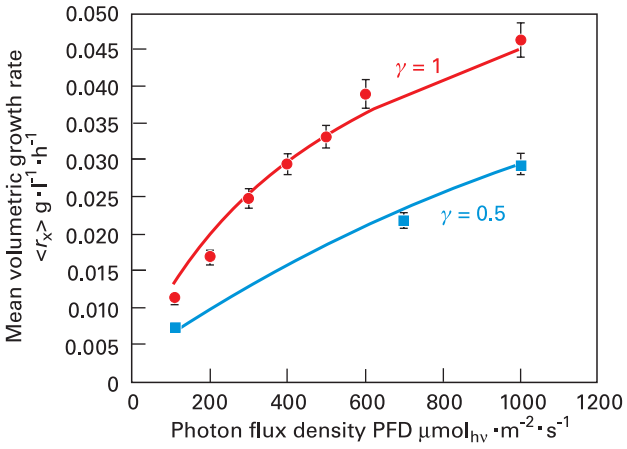

Fig. 10.10: Prediction of PFD influence on resulting biomass productivity (continuous mode) calculated by the model presented. Comparison with experimental results for the green microalga *Chlamydomonas reinhardtii* cultivated in a torus-shaped PBR (L_z = 0.04 m). The negative influence of introducing a dark volume on microalgal growth is illustrated here, with lower productivities when working in full-light absorption (γ = 0.5) than in the case of a luminostat regime (γ = 1) giving maximal biomass productivity) (see Takache et al. 2012).

neering, enabling us to predict the influence of parameters that affect PBR performance profoundly but in a complex manner.

Figure 10.11 illustrates the utility of increasing the specific illuminated surface (or decreasing the culture depth, i.e. $a_{light} = 1/L$ for a flat panel) and PFD to increase volumetric productivity (or biomass concentration, the two being linked). This introduces the basic concepts of PBR intensification, detailed in Fig. 10.12. The utility of working in a thin film ($a_{light} > 100\,m^{-1}$, $L < 0.01$ m) is clearly demonstrated here: compared with usual geometries (a_{light} around $20\,m^{-1}$ for PBR of depth 0.05 m, $0.3\,m^{-1}$ for raceway of depth 0.3 m), two orders of magnitude on volumetric productivity can be gained allowing operators to work in high cell density culture ($C_x > 10\,kg.m^{-3}$). We also note that increasing the PFD will lead to a further increase (but with a decrease in thermodynamic yield, as discussed above). As previously mentioned, this demonstrates the surface productivity as being independent of the specific illuminated surface, emphasizing a specific feature of PBR intensification with the possibility to increase drastically volumetric productivity while maintaining surface productivity (see also Eq. (10.31) combined with Eq. (10.32)).

Generally, one direct utility of process intensification is that it reduces the system size needed to achieve a given production requirement. In the specific context of microalgal cultivation, we also note that several processes have an energy consumption directly linked to the culture volume (pumping, mixing, temperature control, harvesting, etc.). Increasing volumetric productivity can thus drastically

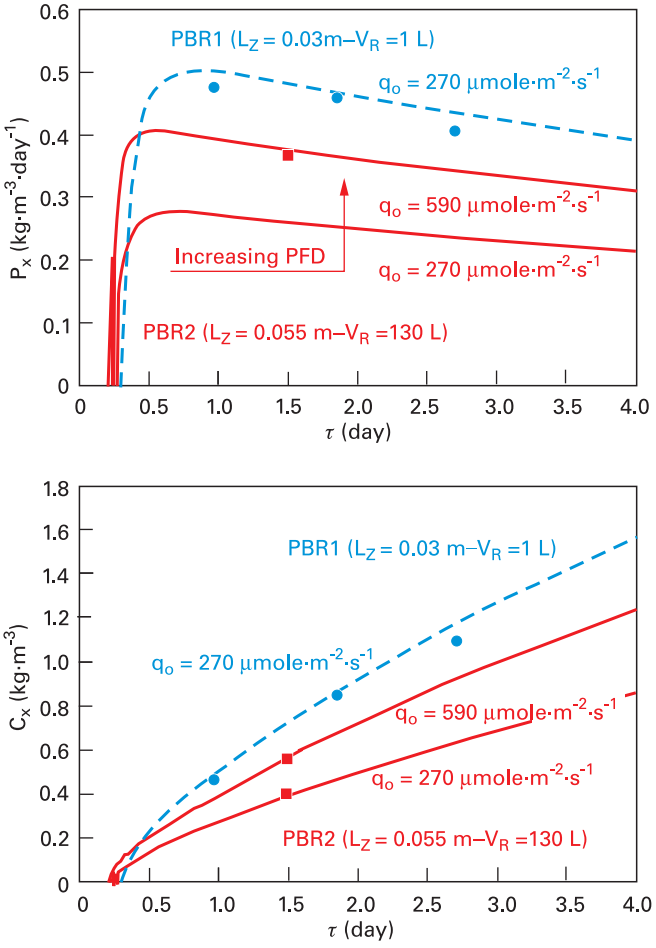

Fig. 10.11: Scaling up of biomass production from laboratory scale 1 L PBR to 130 L PBR with *Neochloris oleoabundans*. The light-limited growth model was used to predict effects of different parameters on productivities or biomass concentration (dashed line for PBR1 and continuous line for PBR2), such as the positive effect of increasing the PFD on biomass productivity, or the negative effect of increasing the depth of culture.

reduce energy needs for a given operation. This is of primary relevance, for example, in biofuel production, where both surface and volumetric productivities can be increased with appropriate engineering of photobioreactors (using, for example, models described in this chapter; the authors are developing optimized systems for solar production by these means).

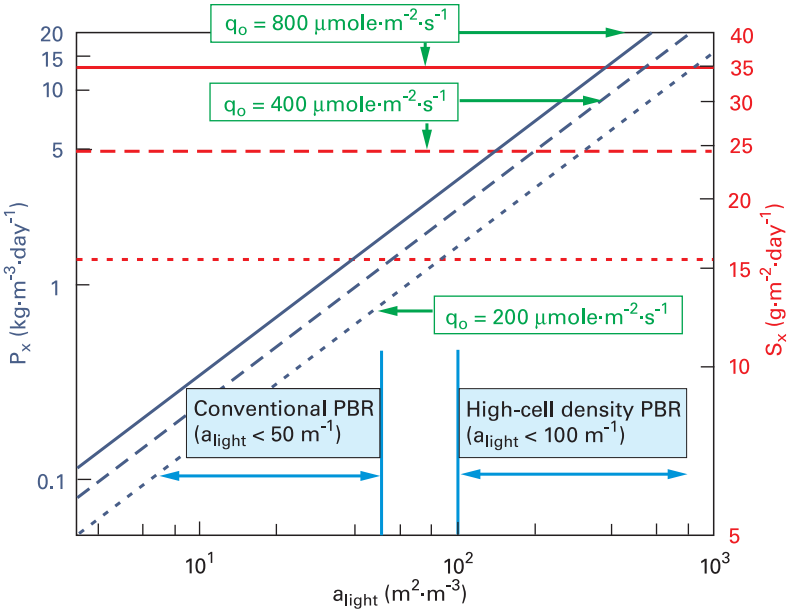

Fig. 10.12: Influence of the illuminated surface-to-volume ratio (a_{light}) on PBR productivities in the case of *Chlamydomonas reinhardtii* cultivation. A direct influence on volumetric productivity is shown (two orders of magnitude of variation). Surface productivity is found independent of this engineering parameter. PFD is found to have a positive effect on both values (all values correspond to maximal performances as obtained in continuous cultivation, light-limited conditions, luminostat "γ = 1" regime).

10.4.1.4 Engineering formula for assessment of maximum kinetic performance in PBRs

Among the many practical advantages of defining an illuminated volume fraction y in the PBR, we note that it enables us to clearly define (at least from a didactic and theoretical point of view) optimal operating conditions for a given geometry of a PBR illuminated with a constant PFD. This means that from a sound control of the radiation field by acting on the biomass concentration guaranteeing the condition $y = 1$ as rigorously as possible, it is possible to achieve the maximal kinetic performance of the PBR $\langle r_X \rangle_{max}$. This also shows that for an existing reactor and fixed PFD, the radiation field may be controlled solely by the biomass concentration C_X (varying the residence time as previously shown), demonstrating why batch cultivations for microalgae should be avoided if maximal performance is sought.

The authors have recently shown (Cornet and Dussap 2009), on many different PBR geometries, that only in the special case $y = 1 \pm 20\,\%$, and accepting an accuracy of around 15 %, is it possible to use a simple engineering formula, already averaged over the total volume of the PBR, in which the complexity of the radiative

transfer has vanished. This very useful relation, with for main parameters the design-specific illuminated area a_{light} and the incident PFD q_0 (here in $\mu\text{mol}_{h\nu}.\text{m}^{-2}.\text{s}^{-1}$) with its degree of collimation n, takes the form:

$$< r_X >_{\max} = (1 - f_d)\,\rho_M\, M_X\, \overline{\varphi}'_X \frac{2\alpha}{1+\alpha} a_{\text{light}} \frac{K}{\left(\frac{n+2}{n+1}\right)} \ln\left[1 + \frac{\left(\frac{n+2}{n+1}\right) q_0}{K}\right] \tag{10.32}$$

in which all the variables have already been defined in this chapter except for f_d, which represents the dark fraction of the reactor (any volume fraction of the PBR not lit by the incident PFD). In this equation, the only specific parameters of a given micro-organism are the linear scattering modulus α (default value 0.9), the molar mass M_X (default value 0.024 kg$X$/mol$X$) and the half saturation constant for photosynthesis K (default value 100 $\mu\text{mol}_{h\nu}.\text{m}^{-2}.\text{s}^{-1}$). This formula, originally validated for cyanobacteria, also proved very robust for microalgae (Takache et al. 2010).

10.4.2 Solar production

10.4.2.1 Prediction of PBR productivity as a function of radiation conditions

Generally, in the current perspective of using mass scale production of algae as a new feedstock source for various applications, predicting productivity is obviously useful (productivity calculations, cultivation system engineering, advanced control settings, etc.). However, the broad variability of sunlight in time and space adds further complexity to the optimization and control of cultivation systems, compared with artificial illumination. Modeling can be very helpful in this regard, and the approach was recently extended by the authors to that end by considering specific features of solar use such as (1) direct/diffuse radiation proportions in sunlight, and (2) time variation of the incident light flux and corresponding incident angle on the surface of the cultivation system. All these variables can be obtained from a solar database giving time (day/night, season) and space variability of solar radiation. They can then be implemented in a PBR model, using the same approach as described above. Besides the specific nature of sunlight (non-normal incident angle, non-negligible diffuse radiation), an important difference lies in the transient nature of sunlight. The transient form of the mass balance equation thus has to be solved (this can be achieved using the routine *ode23tb* in the Matlab® software), ultimately allowing the determination of the biomass concentration time course and calculation of the corresponding biomass productivity.

Once the model has been set up, it enables us to link various interacting parameters (irradiation, PBR technology and implementation) and phenomena

(light transfer in the culture bulk, growth kinetics). In solar conditions, where light is highly variable in quality and quantity, this is of critical importance. It allows a deeper understanding of solar PBR transient behavior, and various parameters can be easily investigated (PBR location, but also harvesting strategy, strains cultivated, effect of night, etc.). Production can also be determined for a whole-year period, giving data such as productivity, obviously difficult to obtain in real conditions (at least for reasons of time). An example of surface productivity is given in Figure 10.13 (a surface productivity is especially useful in the context of solar production to determine the required land area). Two locations were investigated by introducing adequate irradiation conditions, namely Dongola (Africa), here retained for its irradiation conditions close to the maximum available anywhere on Earth (around 2500 $kWh.m^{-2}.year^{-1}$), and Nantes, with typical irradiation conditions of western Europe (around 1220 $kWh.m^{-2}.year^{-1}$). The direct relation between irradiation conditions and biomass productivities is shown, with variations along the year, especially in Nantes, where a threefold increase is observed between winter and summer periods. Simulation obviously allows further analysis (influence of day/night duration, influence of cloudy days, effect of high irradiation conditions as obtained in the summer, etc.). This, however, lies outside the scope of this chapter; the interested reader can refer to the authors' work on the subject (Pruvost et al. 2011b for biomass production; Goetz et al. 2011 for thermal behavior prediction).

Another advantage of modeling is the possibility it offers of calculating theoretical limits independently of practical constraints (which will inevitably lower productivities). This can be done, as recently illustrated by the authors, by introducing ideal conditions in the model. The concept of ideal reactor was introduced, as commonly done in chemical engineering (Aris 1999), by calculating maximal productivity for the light-limited regime and for an optimal running of the PBR with the ideal solar condition that could be achieved on Earth. This allows an estimate of the upper limit of biomass productivity for *A. platensis* cultivated on nitrate from a kinetic approach (calculation of $\langle r_X \rangle$ and $\langle s_X \rangle$ from the proposed coupling models), added to the previously described energetic approach (for a species growing on ammonia, 25 % higher productivity should be expected). For a fix surface-lightened PBR, we found an excellent agreement with the previous thermodynamic approach, a maximal surface productivity of around 40 $t_X.ha^{-1}.year^{-1}$ being obtained (Pruvost et al. 2012). Because of their difference in light-use principle (light dilution), volumetric-lightened systems with optimal internal light dilution enabled us to approach the thermodynamic limit of photosynthetic reactive systems (see Section 10.3.5), leading to an ideal productivity of 320 $t_X.ha^{-1}.year^{-1}$. By definition, ideal productivity represents an upper limit that cannot be exceeded, irrespective of the technology used. Any real system will have lower productivity due to:

- non-ideal irradiation conditions such as induced by the location, meteorological conditions, partial shading by other units or surrounding buildings or trees, etc.;

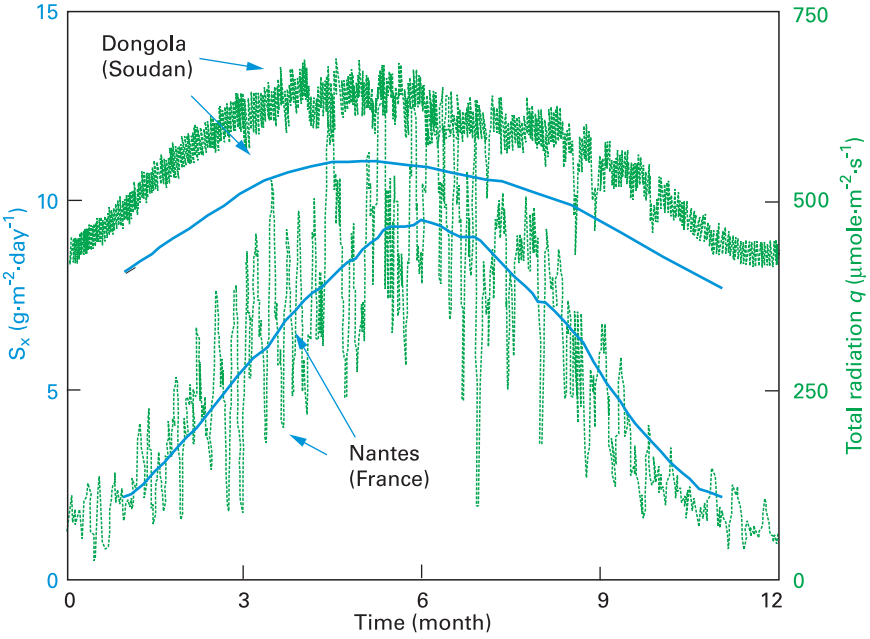

Fig. 10.13: Annual time course of surface productivity (month averaging) of a horizontal PBR located in Dongola (Soudan, 19.1° N, 30.3° W) and Nantes (France, 47° 12′ N, 01° 33′ W). Values are for a system cultivating *Arthrospira platensis* in chemostat mode (optimal residence time). Corresponding radiation time course is also given. Modeling allows the determination of annual averaged productivity as a function of location (in this case, average productivities of 9.5 g.m^{-2}.day^{-1} and 5.5 g.m^{-2}.day^{-1} are expected in Dongola and Nantes respectively due to the difference in radiation conditions).

- the transient response of the PBR resulting from biological kinetics, daytime variation of irradiation and night periods;
- poor control of the radiation field, leading, for example, to a kinetic regime;
- any engineering (PBR orientation and inclination, dark volumes in the system, arrangement of modules and self-shadowing), technical (optical transmittances, etc.) or operating constraints (non-ideal temperature or pH, non-optimized harvesting strategies, contamination, etc.) resulting in non-ideal production conditions.

Practical constraints can be introduced in the model so that their respective contributions to process performance can be quantified. Again, modeling proves to be a highly valuable tool in the systematic engineering and optimization of complex processes such as solar microalgal production systems.

10.4.2.2 Engineering formula for maximal productivity determination

As explained earlier in this chapter, the authors have demonstrated that it is possible to derive a simple engineering formula with constant artificial illumination conditions on a PBR of any given geometry in order to calculate its maximum kinetic performance (Cornet and Dussap 2009; Takache et al. 2010). This approach was recently extended to the case of a mean yearly solar illumination for which it was possible to calculate (for ideal case) or find in databases (for example Meteonorm anywhere in the world) the mean direct $\bar{q}_{//}$ and diffuse $\bar{q}_{\cap}$ PFD (from the knowledge of total PFD $\bar{q}$ and its diffuse fraction $\bar{x}_d$), together with the yearly averaged incidence angle $\overline{\cos\theta}$ with the outward normal of the PBR for the direct illumination (maximal theoretical value of $2/\pi = 0.64$ at the Equator). The maximum surface productivity is then given, for any micro-organism, from the value of the quantum yield $\bar{\varphi}'_X$ on nitrate or ammonium as N-source by the simple relation:

$$< s_X >_{\max} = (1 - f_d)\,\rho_M\, M_X\, \bar{\varphi}'_X \frac{2\alpha}{1+\alpha}\left[\frac{\bar{x}_d K}{2}\ln\left[1 + \frac{2\,\bar{q}}{K}\right] + (1 - \bar{x}_d)\,\overline{\cos\theta}\,K\ln\left[1 + \frac{\bar{q}}{K\,\overline{\cos\theta}}\right]\right] \tag{10.33}$$

As it is related to maximum performance, this equation holds only in optimal running conditions (optimal operation of the cultivation system). However, it proved to give a good engineering estimation of maximum annual achievable productivity from the knowledge only of some kinetic parameters and yearly averaged incident radiation conditions. For example, the deviation, compared with the full simulated values, was found to be below 10 %, confirming the relevance of the proposed formula in the estimation of maximum performance of PBRs (Pruvost et al. 2012).

10.4.3 Modeling light/dark cycle effects

Although many studies have shown the relevance of mixing conditions in microalgal cultivation systems, knowledge is still insufficient to provide engineering rules for their systematic optimization. Hydrodynamic conditions can have several outcomes: some are common to other bioprocesses (hydrodynamic shear stress, mass- and heat-transfer enhancement, cell sedimentation and biofilm formation), while others are specific to microalgal cultivation systems. This is especially so for the light–dark (L/D) cycle effects. In view of their specificity to microalgal cultivation, a brief overview of actual approaches to modeling L/D cycle effects is now presented.

L/D cycles result from cell displacement in the heterogeneous radiation field, so that cells experience a specific history with respect to the light they absorb, composed of variations from high irradiance level (in the vicinity of the light source) to low or quasi-nil values (deep in the culture) if the biomass concentration

is high. As widely described in the literature (Janssen et al. 2000; Richmond 2004; Perner-Nochta and Posten 2007; Rosello Sastre et al. 2007; Pruvost et al. 2008), this dynamic fluctuating regime can influence photosynthetic growth and thereby process efficiency.

Some examples can be found in the literature on the characterization of light regimes in cultivation systems. Firstly, cell trajectories are determined using a schematic representation of the flow (Wu and Merchuk 2002; Janssen et al. 2003; Wu and Merchuk 2004), by experimental measurement with radiative particle tracking (Luo et al. 2003; Luo and Al-Dahhan 2004) or by a Lagrangian simulation (Pruvost et al. 2002a, 2002b). In this last case, trajectories are obtained from the PBR flow-field description. If microalgal cells are assumed to be passive tracers and are represented by elementary fluid particles (no mass effect, as their density is almost the same as that of the fluid, cell size smaller than the Kolmogorov scale), trajectories are then obtained step by step by calculating the successive positions, P, of a fluid element, using:

$$P(t + \Delta t) = P(t) + U_P \, \Delta t \tag{10.34}$$

where U_P is the instantaneous velocity at a given position P and Δt a time step to be specified.

The velocity field can be determined using computational fluid dynamics (CFD). For a laminar regime, the velocity field then obtained is fully determined, and a direct calculation can be made. However, in most cases, a turbulent regime will be encountered. Due to the fluctuating nature of the velocity, a specific formulation will be required to consider turbulent effects on cell dispersion (using, for example, a stochastic model; see Pruvost et al. 2008).

Once cell trajectories are known, the light regime is then obtained by introducing the radiative transfer model. However, as shown in Pruvost et al. (2008), attention must be paid to the formulation of the coupling. Mixing can influence the spatial distribution of particles participating in radiative transfer, resulting in a non-linear modification of the radiation field (Cassano et al. 1995). The calculation method for the radiative transfer has thus to be modified to take into account the effect of non-ideal mixing conditions. An oversimplified formulation (as usually proposed), where cell trajectories and radiative transfer are solved independently, results in a wrong formulation of the Lagrangian characterization of light regimes encountered by flowing cells in the PBR. This false representation of light availability in the reactor can lead to a significant overestimation of the L/D cycle effects on resulting growth (by increasing light received by algae, leading to an energy imbalance contravening the first law of thermodynamics). A correction of radiative transfer with respect to the time spent by flowing cells along the depth of culture is necessary here.

Typical results of cell trajectories obtained using a Lagrangian approach are given in Figure 10.14. These results emphasize the rapid variations in light intensity

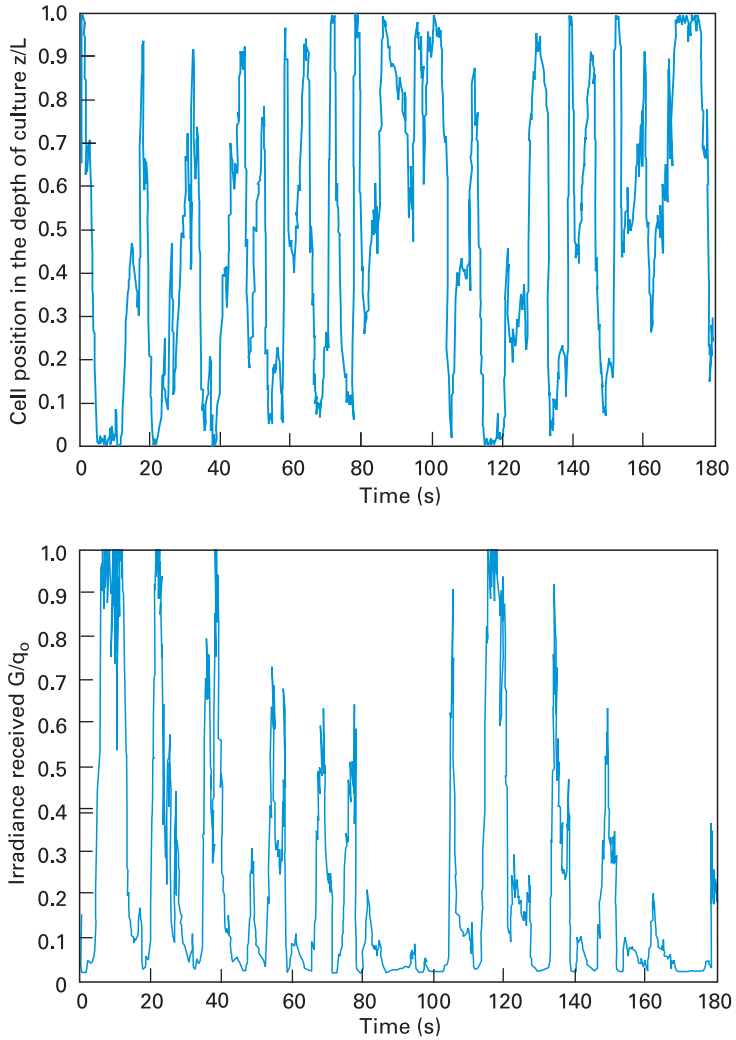

Fig. 10.14: Example of cell displacement along the light gradient (left) and corresponding light/dark cycles (right). Results were obtained here for a torus-shaped PBR with mechanical mixing (marine impeller). The flow field was determined using CFD. Cell trajectories from a Lagrangian approach were combined with radiative transfer modeling (corrected here to obtain an energetically consistent formulation) to calculate the resulting light regime. See Pruvost et al. (2008) for details.

when cells flow along the light gradient (the example is given here for a torus-shaped PBR mixed with a marine impeller). If there is a dynamic kinetic coupling between biological response and fluctuating light regimes encountered by flowing cells (the L/D cycle effect), PBR efficiency will be modified due to the non-linearity thereby added to light conversion. As it allows cell history to be represented, the

further coupling of the Lagrangian approach (with a rigorous treatment of the radiative transfer problem, as previously discussed) with kinetic models of photosynthesis is direct. This opens perspectives to adapt light regimes in PBRs with respect to biological response timescales (especially when using CFD, which allows various hydrodynamic conditions to be simulated, such as modification of flow rate, aeration or impeller rotation speed). Formulation of a kinetic model of photosynthetic growth able to represent L/D cycle effects is, however, far from trivial, L/D cycles being widely distributed in frequency and magnitude, with effects strongly dependent on the cultivated species. It is also not totally clear at what level L/D cycles interfere in the metabolism. Effects have been reported on the alteration of instantaneous photosynthetic conversion (Kok effect), but also photoacclimation with progressive pigment modifications (Janssen et al. 1999, 2000). Some attempts to devise dynamic models can be found in the literature (Pahl-Wostl 1992; Eilers and Peeters 1993; Wu and Merchuk 2001, 2002; Camacho et al. 2003; Luo and Al-Dahhan 2004; Wu and Merchuk 2004; Yoshimoto et al. 2005), but more work is still clearly needed to develop robust, generalizable dynamic models. Optimization and modeling of L/D cycle effects in microalgal cultivation systems thus await further research efforts.

10.5 Acknowledgments

This book chapter is the result of many years of collaborative work. The authors thank all their colleagues and PhD students involved in this long-term ongoing research effort. This work was also supported by several French and European research programs (ANR BIOSOLIS, SHAMASH, ALGOH2, SOLARH2).

10.6 Nomenclature

a	Volumetric absorption coefficient (m^{-1})
a_{light}	Specific illuminated area for any given photobioreactor (m^{-1})
$\mathcal{A}$	Specific local volumetric radiant power density absorbed ($\mu mol.s^{-1}.kg^{-1}$ or $W.kg^{-1}$)
b_λ	Back-scattered fraction for radiation of wavelength λ (dimensionless)
$C_{(j)}$	Mass concentration (for species j) ($kg.m^{-3}$ or $g.L^{-1}$)
C_X	Biomass concentration ($kg.m^{-3}$ or $g.L^{-1}$)
D	Dilution rate of the photobioreactor (s^{-1} or h^{-1})
D_L	Coefficient of axial dispersion ($m^2.s^{-1}$)
E_a	Mass absorption coefficient ($m^2.kg^{-1}$)
E_s	Mass scattering coefficient ($m^2.kg^{-1}$)
f_d	Design dark volume fraction of any photobioreactor (dimensionless)
G	Local spherical irradiance ($W.m^{-2}$ or $\mu mol.s^{-1}.m^{-2}$)

G_C Local spherical irradiance for compensation point ($W.m^{-2}$ or $\mu mol.s^{-1}.m^{-2}$)
I Specific radiant intensity ($W.m^{-2}.sr^{-1}$ or $\mu mol.s^{-1}.m^{-2}.sr^{-1}$)
J_i Molar specific rate for species i ($mol(i).kg\ X^{-1}.s^{-1}$)
K Half saturation constant for photosynthesis ($W.m^{-2}$ or $\mu mol.s^{-1}.m^{-2}$)
K_r Saturation constant for respiration inhibition at light ($W.m^{-2}$ or $\mu mol.s^{-1}.m^{-2}$)
L Total length of a rectangular photobioreactor (m)
M_X C-molar mass for the biomass ($kg.mol^{-1}$)
$\mathbf{n}$ Outward normal to a surface (dimensionless)
n Degree of collimation for the radiation field (dimensionless)
$p(\mathbf{\Omega}, \mathbf{\Omega}')$ or $p(\beta, \beta')$ Phase function for scattering (dimensionless)
$\mathbf{q}$ Photon (or radiant) flux density ($W.m^{-2}$ or $\mu mol.s^{-1}.m^{-2}$)
q_x Projection of the hemispherical incident photon flux density on a surface perpendicular to the x-axis ($W.m^{-2}$ or $\mu mol.s^{-1}.m^{-2}$)
$q_\cap$ Diffuse hemispherical incident photon flux density (PFD) in the PAR ($W.m^{-2}$ or $\mu mol.s^{-1}.m^{-2}$)
$q_{//}$ Collimated hemispherical incident photon flux density (PFD) in the PAR ($W.m^{-2}$ or $\mu mol.s^{-1}.m^{-2}$)
$q_\perp$ Normally collimated hemispherical incident photon flux density (PFD) in the PAR ($W.m^{-2}$ or $\mu mol.s^{-1}.m^{-2}$)
Q Volume liquid flow rate ($m^3.s^{-1}$ or $m^3.h^{-1}$)
Q_P Photosynthetic quotient (dimensionless)
r_i Mass volumetric rate for species i ($kg.m^{-3}.s^{-1}$ or $kg.m^{-3}.h^{-1}$)
rI Mole volumetric rate for species i ($mol.m^{-3}.s^{-1}$ or $mol.m^{-3}.h^{-1}$)
r_X Biomass volumetric growth rate (productivity) ($kg.m^{-3}.s^{-1}$ or $kg.m^{-3}.h^{-1}$)
R Radius of any photobioreactor (m)
s Volumetric scattering coefficient (m^{-1})
S Surface (m^2)
S_{light} Illuminated surface of any photobioreactor (m^2)
t Time (s or h)
u Liquid velocity ($m.s^{-1}$)
U_P Particle velocity ($m.s^{-1}$)
V Volume (m^3 or L)
V_ℓ Illuminated volume inside the photobioreactor (m^3 or L)
x_d Fraction of diffuse radiation in the total incident solar flux density (PAR) (dimensionless)
x, z x- or z- direction, length (m)
z_C Extinction length corresponding to irradiance of compensation G_C (m)

Greek letters

α Linear scattering modulus for the two-flux model approximation (dimensionless)

β, β' Polar angles (rad)
y Fraction for working illuminated volume in the photobioreactor (dimensionless)
δ Extinction coefficient for the two-flux model approximation (m^{-1})
$\Delta g_i'^{o}$ Standard Gibbs free enthalpy for species i ($J.mol^{-1}$)
η_{th} Thermodynamic efficiency of the photobioreactor (dimensionless)
Θ Polar angle (rad)
θ Polar angle (rad)
λ Wavelength (m)
$\mu = \cos\theta$ (dimensionless)
μ_i Chemical potential for species i ($J.mol^{-1}$)
ρ Energetic yield for photon conversion (dimensionless)
ρ_M Maximum energetic yield for photon conversion (dimensionless)
τ Hydraulic residence time (s or h or days)
τ_λ Optical thickness (dimensionless)
υ_{i-j} Stoichiometric coefficient (dimensionless)
φ_X' Biomass mole quantum yield for the Z-scheme of photosynthesis ($mol\ X.\mu mol_{h\nu}^{-1}$)
φ_{O_2}' Oxygen mole quantum yield for the Z-scheme of photosynthesis ($mol_{O2}.\mu mol_{h\nu}^{-1}$)
φ Azimuth angle (rad)
Φ Azimuth angle (rad)
ω Solid angle (rad)
ϖ_λ Albedo of single scattering for the wavelength λ (dimensionless)
$\mathbf{\Omega}$ Unit directional vector (dimensionless)

Subscripts

0 Relative to the input surface of a rectangular photobioreactor ($u = 0$)
c Relative to the compensation point for photosynthesis
col Relative to collimated radiation
dif Relative to diffuse radiation
i Relative to input quantity
R Relative to the reactor
λ Relative to a spectral quantity for the wavelength λ
max Maximum value for the volumetric productivity r_X

Superscripts

col Relative to collimated radiation
dif Relative to diffuse radiation

Other

$\overline{X} = \frac{1}{\Delta t} \int_{\Delta t} X \, \mathrm{d}t$ Time averaging

$< X > = \frac{1}{V} \iiint_{V} X \, \mathrm{d}V$ Spatial averaging

Abbreviations

CSTR Completely stirred tank reactor
DOM Differential discrete ordinates method
PAR Photosynthetically active radiation
PBR Photobioreactor
PFD Photon flux density
PFTR Plug flow tubular reactor
RTE Radiative transfer equation

References

Aiba, S. 1982. Growth kinetics of photosynthetic microorganisms. *Adv. Biochem. Eng. Biotechnol. 23*, 85–156.

Aris, R. 1999. Elementary Chemical Reactor Analysis. Dover, New York.

Berberoglu, H. and L. Pilon. 2007. Experimental measurements of the radiation characteristics of *Anabaena variabilis* ATCC 29413-U and *Rhodobacter sphaeroides* ATCC 49419. *Int. J. Hydrogen Energy 32*, 4772–4785.

Bidigare, R. R., M. E. Ondrusek, J. H. Morrow and D. A. Kiefer. 1990. *In vivo* absorption properties of algal pigments. *SPIE Ocean Optics X 1302*, 290–302.

Bohren, C. F., D. R. Huffman. 1983. *Absorption and Scattering of Light by Small Particles*. John Wiley and Sons, New York.

Camacho, F. R., F. G. Camacho, F. J. M. Sevilla, Y. Chisti and E. Molina Grima. 2003. A mechanistic model of photosynthesis in microalgae. *Biotechnol. Bioeng. 81* (4), 459–473.

Cassano, A. E., C. A. Martin, R. J. Brandi and O. M. Alfano. 1995. Photoreactor analysis and design: fundamentals and applications. *Ind. Eng. Chem. Res. 34*, 2155–2201.

Chandrasekhar, S. 1960. *Radiative Transfer*. Dover Publications Inc., New York.

Cogne, G., M. Rugen, A. Bockmayr, M. Titica, C. G. Dussap, J. F. Cornet and J. Legrand. 2011. A model-based method for investigating bioenergetic processes in autotrophically growing eukaryotic microalgae: application to the green alga *Chlamydomonas reinhardtii*. *Biotechnol. Prog. 27*, 631–640.

Cornet, J. -F. 2005. Theoretical foundations and covariant balances for chemical engineering applications with electromagnetic field. *Chem. Eng. Commun. 192*, 647–666.

Cornet, J. -F. 2007. Procédés limités par le transfert de rayonnement en milieu hétérogène – Étude des couplages cinétiques et énergétiques dans les photobioréacteurs par une approche thermodynamique. Habilitation à Diriger les Recherches, Université Blaise Pascal Clermont-Ferrand, n°236.

Cornet, J. -F. 2010. Calculation of optimal design and ideal productivities of volumetrically-lightened photobioreactors using the constructal approach. *Chem. Eng. Sci. 65*, 985–998.

Cornet, J. -F., C. G. Dussap, P. Cluzel and G. Dubertret. 1992. A structured model for simulation of cultures of the cyanobacterium *Spirulina platensis* in photobioreactors. I. Coupling between light transfer and growth kinetics. *Biotechnol. Bioeng. 40* (7), 817–825.

Cornet, J. -F., C. G. Dussap and J. -B. Gros. 1994. Conversion of radiant light energy in photobioreactors. *AIChE J. 40*, 1055–1066.

Cornet, J. -F., C. G. Dussap, J. -B. Gros, C. Binois and C. Lasseur. 1995. A simplified monodimensional approach for modeling coupling between radiant light transfer and growth kinetics in photobioreactors. *Chem. Eng. Sci. 50*, 1489–1500.

Cornet, J. -F., C. G. Dussap and J. -B. Gros. 1998. Kinetics and energetics of photosynthetic microorganisms in photobioreactors. Application to *Spirulina* growth. *Adv. Biochem. Eng. Biotechnol. 59*, 153–224.

Cornet, J. -F., L. Favier and C. G. Dussap. 2003. Modeling stability of photoheterotrophic continuous cultures in photobioreactors. *Biotechnol. Prog. 19* (4), 1216–1227.

Cornet, J. -F. and C. G. Dussap. 2009. A simple and reliable formula for assessment of maximum volumetric productivities in photobioreactors. *Biotechnol. Prog. 25*, 424–435.

Cournac, L., F. Musa, L. Bernard, G. Guedeney, P. Vignais and G. Peltier. 2002. Limiting steps of hydrogen production in *Chlamydomonas reinhardtii* and *Synechocystis* PCC 6803 as analysed by light-induced gas exchange transients. *Int. J. Hydrogen Energy 27*, 1229–1237.

Csogör Z., M. Herrenbauer, K. Schmidt and C. Posten. 2001. Light distribution in a novel photobioreactor – modelling for optimization. *J. Appl. Phycol. 13*, 325–333.

Dauchet, J., S. Blanco, J. -F. Cornet, M. El Hafi, V. Eymet and R. Fournier. 2012a. The practice of recent radiative transfer Monte Carlo advances and its contribution to the field of microorganisms cultivation in photobioreactors. *J. Phys. Conf. Ser*. In press.

Dauchet, J., S. Blanco, J. -F. Cornet and R. Fournier. 2012b. Radiative properties of photosynthetic microorganisms. *J. Quant. Spectrosc. Radiat. Transfer*. Submitted.

Degrenne, B., J. Pruvost, G. Christophe, J. -F. Cornet, G. Cogne and J. Legrand. 2010. Investigation of the combined effects of acetate and photobioreactor illuminated fraction in the induction of anoxia for hydrogen production by *Chlamydomonas reinhardtii*. *Int. J. Hydrogen Energy*. In press (available online).

Eilers, P. H. C. and J. C. H. Peeters. 1993. Dynamic behaviour of a model for photosynthesis and photoinhibition. *Ecol. Model. 69*, 113–133.

Farges, B., C. Laroche, J. -F. Cornet and C. G. Dussap, 2009 Spectral kinetic modeling and long-term behavior assessment of *Arthrospira platensis* growth in photobioreactors under red (620 nm) light illumination. *Biotechnol. Prog. 25*, 151–162.

Fouchard, S., J. Pruvost, B. Degrenne, M. Titica and J. Legrand. 2009. Kinetic modeling of light limitation and sulphur deprivation effects in the induction of hydrogen production with Chlamydomonas reinhardtii Part I: Model description and parameters determination. *Biotechnol. Bioeng. 102* (1), 132–147.

Goetz, V., F. Le Borgne, J. Pruvost, G. Plantard and J. Legrand. 2011. A generic temperature model for solar photobioreactors. *Chem. Eng. J. 175*, 443–449.

Gonzalez de la Vara, L. and C. Gomez-Lojero. 1986. Participation of plastoquinone, cytochrome c553 and ferredoxin-NADP+ oxido reductase in both photosynthesis and respiration in *Spirulina maxima*. *Photosynth. Res. 8*, 65–78.

Hottel, H. C. and Sarofim, A. F. 1967. *Radiative Transfer*. McGraw-Hill, New York.

Houf, W. G. and F. P. Incropera. 1980. An assessment of techniques for predicting radiation transfer in aqueous media. *J. Quant. Spectrosc. Radiat. Transfer 23*, 101–115.

Irazoqui, H. A., J. Cerdá and A. E. Cassano. 1976. The radiation field for the point and line source approximations and the three-dimensional source models. Applications to photoreactions. *Chem. Eng. J. 11*, 27–37.

Janssen, M. G. J., T. C. Kuijpers, B. Veldhoen, M. B. Ternbach, J. Tramper, L. R. Mur and Wijffels, R. H. 1999. Specific growth rate of *Chlamydomonas reinhardtii* and *Chlorella sorokiniana* under medium duration light/dark cycles 13–87 s. *J. Biotechnol. 70*, 323–333.

Janssen, M., M. G. J. Janssen, M. De Winter, J. Tramper, L. R. Mur, J. Snel and R. H. Wijffels. 2000. Efficiency of light utilization of *Chlamydomonas reinhardtii* under medium-duration light/dark cycles. *J. Biotechnol. 78*, 123–137.

Janssen, M., J. Tramper, L. R. Mur and R. H. Wijffels. 2003. Enclosed outdoor photobioreactors: Light regime, photosynthetic efficiency, scale-up, and future prospects. *Biotechnol. Bioeng. 81*, 193–210.

Kumar, S., A. Majumdar and C. L. Tien. 1990. The differential-discrete-ordinate method for solutions of the equation of radiative transfer. *J. Heat Transfer 112*, 424–429.

Lucarini, V., J. J. Saarinen, K. -E. Peiponen and E. M. Vartiainen. 2005. *Kramers–Kronig Relations in Optical Materials Research*. Springer-Verlag, Berlin.

Luo, H. P., A. Kemoun, M. H. Al-Dahhan, Fernandez, J. M. Sevilla, J. L. Garcia Sanchez, F. Garcia Camacho and E. Molina Grima. 2003. Analysis of photobioreactors for culturing high-value microalgae and cyanobacteria via an advanced diagnostic technique: CARPT. *Chem. Eng. Sci.* 58, 2519–2527.

Luo, H. P. and M. H. Al-Dahhan. 2004. Analyzing and modeling of photobioreactors by combining first principles of physiology and hydrodynamics. *Biotechnol. Bioeng*. *85*(4), 382–393.

Mattheij, R. M. M. and G. W. M. Staarink. 1984a. An efficient algorithm for solving general linear two-point BVP. *SIAM J. Sci. Stat. Comput. 5*, 745–763.

Mattheij, R. M. M. and G. W. M. Staarink. 1984b. An optimal shooting intervals. *Math. Comput. 42*, 25–40.

Mishchenko, M. I., J. W. Hovenier and L. D. Travis. 2000. *Light Scattering by Nonspherical Particles. Theory, Measurements and Applications*. Academic Press, San Diego, CA.

Myers, J. and K. A. Kratz. 1955. Relation between pigment content and photosynthetic characteristics in blue green algae. *J. Gen. Physiol. 39*, 11–22.

Pahl-Wostl, C. 1992. Dynamic versus static models for photosynthetis. *Hydrobiologia 238*, 189–196.

Peltier, G. and P. Thibault. 1985. Uptake in the light in *Chlamydomonas*. Evidence for persistent mitochondrial respiration. *Plant Physiol*. *79*, 225–230.

Perner-Nochta I. and C. Posten. 2007. Simulations of light intensity variation in photobioreactors. *J. Biotechnol. 131* (3), 276–285.

Pilon, L., H. Berberoglu and R. Kandilian. 2011. Radiation transfer in photobiological carbon dioxide fixation and fuel production by microalgae. *J. Quant. Spectrosc. Radiat. Transfer 112*, 2639–2660.

Pottier, L., J. Pruvost, J. Deremetz, J.-F. Cornet, J. Legrand and C. G. Dussap. 2005. A fully predictive model for one-dimensional light attenuation by *Chlamydomonas reinhardtii* in a torus photobioreactor. *Biotechnol. Bioeng. 91*, 569–582.

Pruvost, J. 2011. Cultivation of algae in photobioreactors for biodiesel production. In: *Biofuels: Alternative Feedstocks and Conversion Processes*. A. Pandey, C. Larroche, S. C. Ricke, C. G. Dussap and E. Gnansounou, eds. Elsevier, Oxford. pp. 439–464.

Pruvost, J., J. Legrand, P. Legentilhomme and A. Muller-Feuga. 2002a. Simulation of microalgae growth in limiting light conditions – flow effect. *AIChE J. 48*, 1109–1120.

Pruvost, J., J. Legrand, P. Legentilhomme and A. Muller-Feuga. 2002b. Trajectory Lagrangian model for turbulent swirling flow in an annular cell. Comparison with RTD measurements. *Chem. Eng. Sci. 57*, 1205–1215.

Pruvost J., J. -F. Cornet and J. Legrand. 2008. Hydrodynamics influence on light conversion in photobioreactors: an energetically consistent analysis. *Chem. Eng. Sci. 63*, 3679–3694.

Pruvost J., G. Van Vooren, B. Le Gouic, A. Couzinet-Mossion and J. Legrand. 2011a. Systematic investigation of biomass and lipid productivity by microalgae in photobioreactors for biodiesel application. *Bioresour. Technol. 102*, 150–158.

Pruvost J., J. -F. Cornet, V. Goetz and J. Legrand. 2011b. Modeling dynamic functioning of rectangular photobioreactors in solar conditions. *AIChE J. 57*, 1947–1960.

Pruvost J., J. -F. Cornet, V. Goetz and J. Legrand. 2012. Theoretical investigation of biomass productivities achievable in solar rectangular photobioreactors for the cyanobacterium *Arthrospira platensis*. *Biotech. Prog*. In press.

Richmond, A. 2004. Handbook of Microalgal Culture: Biotechnology and Applied Phycology. Blackwell Sciences, Oxford.

Roels, J. A. 1983. *Energetics and Kinetics in Biotechnology*. Elsevier Biomedical Press, Amsterdam.

Rosello Sastre, R., Z. Csögör, I. Perner-Nochta, P. Fleck-Schneider and C. Posten. 2007. Scale-down of microalgae cultivations in tubular photo-bioreactors – A conceptual approach. *J. Biotechnol. 132* (2), 127–133.

Schuster, A. 1905. Radiation through a foggy atmosphere. *Astrophys. J*. 21, 1–21.

Siegel, R. and J. R. Howell. 2002. *Thermal Radiation Heat Transfer*. 4th Edition. Taylor & Francis, New York.

Spadoni, G., E. Bandini and F. Santarelli. 1978. Scattering effects in photosensitized reactions. *Chem. Eng. Sci. 33*, 517–524.

Takache, H., G. Christophe, J.-F. Cornet and J. Pruvost. 2010. Experimental and theoretical assessment of maximum productivities for the micro-algae *Chlamydomonas reinhardtii* in two different geometries of photobioreactors. *Biotechnol. Prog. 26*(2), 431–440.

Takache, H., J. Pruvost and J.-F. Cornet. 2012. Kinetic modeling of the photosynthetic growth of *Chlamydomonas reinhardtii* in photobioreactor. *Biotechnol. Prog*., in press.

Van de Hulst, H. C. 1981. *Light Scattering by Small Particles*. 2nd Edition. Dover Publications Inc., New York.

Vonshak, A. and G. Torzillo. 2004. Environmental stress physiology. In: *Handbook of Microalgal Culture: Biotechnology and Applied Phycology*. A. Richmond, ed. Blackwell Sciences, Oxford. pp. 57–82.

Wu, X., Merchuk, J. C. 2001. A model integrating fluid dynamics in photosynthesis and photoinhibition processes. *Chem. Eng. Sci. 56*, 3527–3538.

Wu, X., Merchuk, J. C. 2002. Simulation of algae growth in a bench-scale column reactor. *Biotechnol. Bioeng. 80* (2), 156–168.

Wu, X., Merchuk, J. C. 2004. Simulation of algae growth in a bench-scale internal loop airlift reactor. *Chem. Eng. Sci. 59*, 2999–2912.

Yoshimoto, N., T. Sato and Y. Kondo. 2005. Dynamic discrete model of flashing light effect in photosynthesis of microalgae. *J. Appl. Phycol. 17* (3). 207–214.

Yun, Y. S. and J. M. Park. 2003. Kinetic modeling of the light-dependent photosynthetic activity of the green microalga *Chlorella vulgaris*. *Biotech. Bioeng. 83*, 303–311.